

# PIM-DL: Expanding the Applicability of Commodity DRAM-PIMs for Deep Learning via Algorithm-System Co-Optimization

Cong Li  
School of Integrated Circuits  
Peking University  
Beijing, China  
leesou@pku.edu.cn

Zhe Zhou  
School of Integrated Circuits  
School of Computer Science  
Peking University  
Beijing, China  
zhou.zhe@pku.edu.cn

Yang Wang\*  
Microsoft Research  
Beijing, China  
yang.wang92@microsoft.com

Fan Yang  
Nankai University  
Tianjin, China  
yangf@nbjl.nankai.edu.cn

Ting Cao  
Microsoft Research  
Beijing, China  
ting.cao@microsoft.com

Mao Yang  
Microsoft Research  
Beijing, China  
maoyang@microsoft.com

Yun Liang  
School of Integrated Circuits  
Peking University  
Beijing Advanced Innovation Center  
for Integrated Circuits  
Beijing, China  
ericlyun@pku.edu.cn

Guangyu Sun\*  
School of Integrated Circuits  
Peking University  
Beijing Advanced Innovation Center  
for Integrated Circuits  
Beijing, China  
gsun@pku.edu.cn

## Abstract

DRAM-based processing-in-memory (DRAM-PIM) has gained commercial prominence in recent years. However, their integration for deep learning acceleration poses inherent challenges. Existing DRAM-PIMs are limited in computational capabilities, primarily applicable for element-wise and GEMV operators. Unfortunately, these operators contribute only a small portion of the execution time in most DNN workloads. Current systems still necessitate powerful hosts to handle a significant portion of compute-heavy operators.

To expand the applicability of commodity DRAM-PIMs in accelerating deep learning, we introduce a novel PIM-DL framework. The philosophy behind PIM-DL is to replace

the compute-heavy GEMM operations in linear layers with Lookup-Tables (LUTs). Such LUT-based neural networks (LUT-NNs) substantially reduce multiplications in DNN inference, rendering them suitable for efficient execution on DRAM-PIMs. To accurately convert DNNs into LUT-NNs and achieve optimal inference serving performance, we first introduce an enhanced LUT-NN (eLUT-NN) algorithm for model calibration, then we propose an Auto-Tuner capable of optimizing the mapping parameters on diverse DRAM-PIM platforms. We evaluate PIM-DL on off-the-shelf UPMEM PIM-DIMM products and simulated HBM-PIM/AiM platforms across multiple contemporary DNN workloads. Compared with GEMM-based inference on DRAM-PIMs, PIM-DL achieves  $22.6\times\sim 37.1\times$  speedup. Compared with CPU/GPU-based inference, PIM-DL achieves up to  $3.54\times/1.20\times$  speedup.

\*Co-corresponding authors.

Permission to make digital or hard copies of all or part of this work for personal or classroom use is granted without fee provided that copies are not made or distributed for profit or commercial advantage and that copies bear this notice and the full citation on the first page. Copyrights for components of this work owned by others than the author(s) must be honored. Abstracting with credit is permitted. To copy otherwise, or republish, to post on servers or to redistribute to lists, requires prior specific permission and/or a fee. Request permissions from [permissions@acm.org](mailto:permissions@acm.org).  
*ASPLOS '24, April 27-May 1, 2024, La Jolla, CA, USA*

© 2024 Copyright held by the owner/author(s). Publication rights licensed to ACM.

ACM ISBN 979-8-4007-0385-0/24/04...\$15.00  
<https://doi.org/10.1145/3620665.3640376>

**CCS Concepts:** • Computing methodologies → Machine learning.

**Keywords:** near-memory processing, machine learning

## ACM Reference Format:

Cong Li, Zhe Zhou, Yang Wang, Fan Yang, Ting Cao, Mao Yang, Yun Liang, and Guangyu Sun. 2024. PIM-DL: Expanding the Applicability of Commodity DRAM-PIMs for Deep Learning via Algorithm-System Co-Optimization. In *29th ACM International Conference on Architectural Support for Programming Languages and Operating Systems, Volume 2 (ASPLOS '24), April 27-May 1, 2024, La Jolla, CA, USA*. ACM, New York, NY, USA, 18 pages. <https://doi.org/10.1145/3620665.3640376>

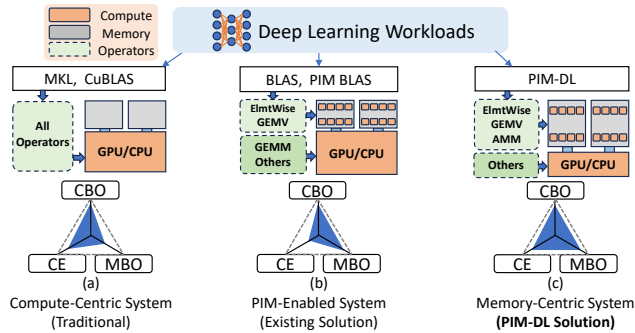


**Figure 1.** Systems Comparison. CBO: Compute-Bound Operators, MBO: Memory-Bound Operators, CE: Cost-Efficiency.

## 1 Introduction

In recent years, commodity DRAM-based processing-in-memory products, exemplified by UPMEM’s PIM-DIMM [18], Samsung’s HBM-PIM [55], and SK-Hynix’s AiM [54], have emerged to enhance DRAM bandwidth while minimizing the data-movement energy consumption. By incorporating processing units near memory banks, these DRAM-PIMs can offer up to  $8\times$  higher memory bandwidth and facilitate the processing of various real-world applications such as in-memory databases [6–8, 48, 62], sparse tensor algebra [31], classic machine learning [34], and genome analysis [21, 58], etc. While DRAM-PIMs have found utility in deep learning applications, their focus primarily lies in memory-intensive layers such as element-wise and GEMV operators [13, 59]. Nevertheless, for typical DNN workloads, element-wise operators only contribute less than 15% of the end-to-end latency [23], while GEMV operators are predominantly utilized in single-batch GPT/LSTM inference [13, 59]. For contemporary DNN serving scenarios in cloud, it is the GEMM operators within linear layers that pose the main bottlenecks [23]. However, none of these DRAM-PIM products have demonstrated the ability to efficiently handle GEMM operators in DNNs.

A primary limitation of DRAM-PIMs in deep-learning acceleration is their restricted computational ability. As DRAM-PIMs implement compute units using the DRAM process, the transistors are  $3\times$  slower, and the logic density is several times lower compared to CMOS in the same technology node [19]. Even worse, DRAM chips usually have fewer metal layers, leading to a lower routing density at the same time. Due to these technical constraints, DRAM-PIMs can hardly incorporate powerful compute units. Consequently, the peak computational capacity of UPMEM PIM-DIMM is merely 43.8 GOP/s per DIMM [33]. Samsung’s HBM-PIM [55] and SK hynix’s GDDR-PIM (AiM) [54] equip dedicated vector units to enhance their tensor-processing ability. HBM-PIM has about 2 TB/s of bandwidth but only 1.2 TFLOP/s of computing capability per cube [55]. Similarly, using high-frequency MAC units, SK-Hynix’s AiM reaches about 1 TFLOP/s per chip. However, the GEMM operators widely used in DNNs

usually require more than 10 TOP/s of computational capacity to ensure sufficient throughput[47]. Therefore, DRAM-PIMs are extremely compute-bound and only applicable for memory-bound operators, such as ReLU [68], Residual [36], Layer-norm [5] and Matrix-Vector Multiplication, etc [59].

To compensate for the limited computational ability, existing PIM-enabled systems (Figure 1-(b)) heavily rely on powerful hosts to handle compute-heavy GEMM operators. Although this improves overall performance, it also leads to higher manufacturing costs. Moreover, due to the majority of computation still happening on the host processors, the utilization of DRAM-PIMs becomes too low to motivate the adoption of DRAM-PIMs in modern data-center systems.

To extend the applicability of DRAM-PIMs for deep-learning, we urgently require a PIM-friendly deep-learning paradigm. In this context, the emerging LUT-NN (Lookup Table-based Neural Network) algorithm [84] becomes a promising solution. It substitutes GEMM in linear layers with table lookups, avoiding extensive multiplications. However, there are three fundamental challenges hindering the application of LUT-NNs on DRAM-PIMs. First, existing LUT-NN algorithms fail to provide satisfactory model accuracy when replacing all linear layers in a DNN with LUTs. Second, current deep learning frameworks do not support DRAM-PIMs as the hardware backend. Third, due to the architectural limitations present in existing DRAM-PIMs, translating the advantages of LUT-NNs into actual speedup is also challenging.

In this paper, we introduce the PIM-DL framework to tackle these challenges. PIM-DL mainly focuses on the optimization of Transformer-based DNNs [87], the de-facto approach in computer vision (CV) and neural language processing (NLP) areas. PIM-DL incorporates a LUT-NN conversion front-end that transforms pre-trained DNNs to LUT-NNs through calibration. The converted models can be efficiently deployed on commodity DRAM-PIMs using a LUT-NN inference backend. To ensure model accuracy, we introduce the enhanced LUT-NN (eLUT-NN) algorithm for efficient model calibration. Unlike baseline LUT-NN algorithms, eLUT-NN can replace all layers with LUTs using only less than 1% of the calibration dataset. To translate the computation reduction achieved by LUT-NNs into actual speedup on DRAM-PIMs, we elaborate the hardware mapping of LUT-NN inference and quantitatively model the dataflow. Then, we develop an auto-tuner to find the best mapping automatically. As shown in Figure 1-(c), PIM-DL enables offloading most operators to DRAM-PIMs and only requires a wimpy host for the small portion of the remaining operators. Compared to the PIM-enabled solution in Figure 1-(b), such a memory-centric system can potentially achieve higher cost-efficiency. To summarize, we have made the following contributions:

- We propose PIM-DL, the first deep-learning framework designed for commodity DRAM-PIMs using the novel LUT-based deep-learning paradigm. (Section 4.1)

- We propose an enhanced LUT-NN (eLUT-NN) algorithm for model calibration, which achieves much higher model accuracy with 100× fewer calibration data. (Section 4.2)
- We design the mapping of LUT-NN on DRAM-PIMs and quantitatively model the dataflow. An auto-tuning framework is proposed to optimize the mapping on different DRAM-PIM platforms. (Section 5)

We evaluate PIM-DL on the off-the-shelf UPMEM PIM-DIMM platform and simulated HBM-PIM/AiM platforms. Compared with GEMM-based inference on PIM-DIMM/HBM-PIM/AiM, PIM-DL achieves up to 22.57×/37.06×/27.25× speedup. Compared with CPU/GPU baselines, PIM-DL achieves up to 3.54×/1.20× speedup. PIM-DL is open-sourced at <https://github.com/leesou/PIM-DL-ASPLOS>.

## 2 Background & Motivation

### 2.1 Memory-Centric Computing with DRAM-PIMs

To deal with the well-known "Memory-Wall" problem, researches have proposed DRAM-based in-memory processing architectures (DRAM-PIMs) over the past decades [2–4, 25, 27, 28, 35, 37, 38, 50, 52, 56, 60, 63, 75, 77, 80, 90, 91, 94, 96, 101]. In recent few years, DRAM-PIMs have entered the commercialization phase, as demonstrated by various products listed in Table 1. Notably, UPMEM has introduced the first DDR4-PIM product named PIM-DIMM [18]. They place programmable RISC cores near every DRAM memory bank, resulting in a remarkable 8× increase in total bandwidth. Additionally, Samsung has proposed HBM-PIM products [55], designed to efficiently process memory-bound basic linear algebra subprograms (BLAS) that do not benefit from on-chip cache, such as scalar-vector, vector-vector, and matrix-vector operations. SK-Hynix has also developed their PIM product named AiM, based on GDDR6 memory, which exhibits significant potential in accelerating LSTM models [54].

### 2.2 Limited Computation Ability of DRAM-PIMs

Commodity DRAM-PIMs have exhibited outstanding performance in accelerating a wide range of workloads [6–8, 21, 31, 48, 58, 62]. Despite these achievements, their application in deep learning remains an open challenge. Prior efforts have employed HBM-PIM [59] and AiM [13] to offload specific types of operators, such as ReLU, Residual, Batch Normalization, and GEMV. However, these element-wise operators typically contribute only < 15% of the overall execution time [23]. Furthermore, while HBM-PIM and AiM can accelerate single-batch GPT/LSTM inference, which primarily involves GEMV operators for linear layers, cloud-based scenarios often require batched inference [24, 29, 47, 81, 103] and heavily rely on compute-heavy GEMM operators. Consequently, existing DRAM-PIM systems still depend on a powerful host to handle these computation-heavy parts in DNNs. We refer to these systems as *PIM-enabled Systems*,

**Table 1.** Comparison of Commodity DRAM-PIMs

Product	PIM-DIMM [18]	HBM-PIM [55]	AiM [54]
Technique	DDR4	HBM2	GDDR6
PIM Units	RISC Cores	FP16 MAC	BF16 MAC
Peak Bandwidth	80.4 GB/s per DIMM	2 TB/s per cube	1 TB/s per chip
Peak Throughput	43.8 GOP/s per DIMM	1.2 TFLOPS	1 TFLOPS

as illustrated in Figure 1-(b). When the workloads are not PIM-friendly, a PIM-enabled system falls back to a traditional compute-centric system shown in Figure 1-(a), but with higher manufacturing costs.

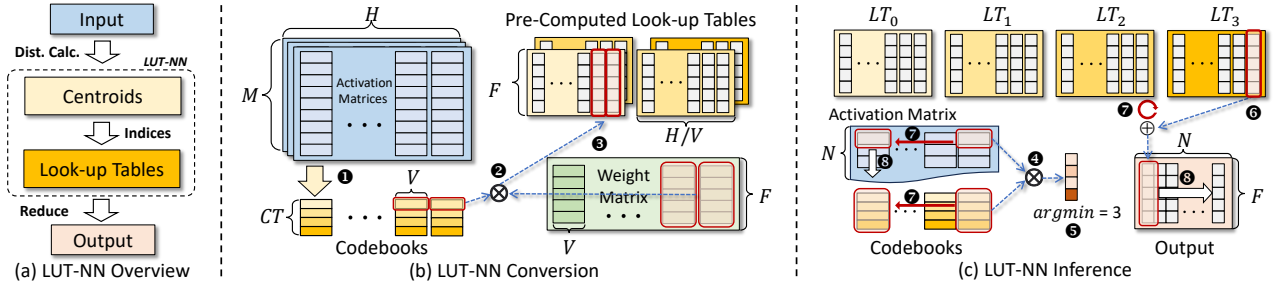
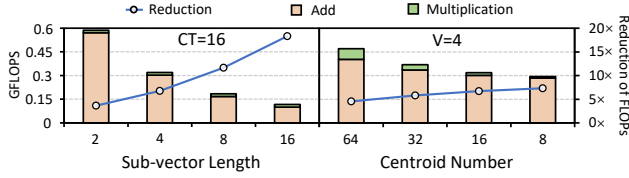
To extend the applicability of commodity DRAM-PIMs for deep learning, a possible direction is to make DNNs more PIM-friendly by reducing their computational requirements. For instance, Prangon et al. [16] proposes to convert CNNs to binary neural networks [66] to enable their deployment on UPMEM’s PIM-DIMM. However, BNNs reduce computation at the cost of greatly sacrificed model accuracy, which can hardly be applied to large models such as BERT [20] and ViT [22] models. Therefore, how to design a practical and PIM-friendly DNN algorithm is yet to be explored.

## 3 LUT-based Deep Learning Paradigm

Compute-heavy GEMM operations have been identified as the primary bottleneck for DNN inference on commodity DRAM-PIMs. Apparently, such a challenge is eliminated if we can substitute GEMM operators with lighter alternatives. In this context, the recently proposed LUT-NN algorithms emerge as a promising solution [9, 84]. The key insight of LUT-NN is that for a given layer, the features of different input activation matrices have block-wise semantic similarity, allowing a few typical features, also named *centroids*, to approximate the original values. Accordingly, the GEMM between any inputs and the weight matrix can be converted to the multiplication between centroids and the weight matrix. By getting the centroids in advance, the partial-sums between the centroids and the weight matrix can be pre-computed and stored in *look-up tables* (LUTs). During inference, we just need to fetch and accumulate the pre-computed data in the LUTs according to the indices of the centroids closest to the inputs, as illustrated in Figure 2-(a). Such a partial-sum reduction procedure can greatly reduce the computation overheads compared with GEMM operators. In the following sub-sections, we will first elaborate on LUT-NN’s conversion and inference procedure. Then, we will analyze the the affinity between LUT-NN and DRAM-PIMs.

### 3.1 LUT-NN Conversion

As shown in Figure 2-(b), LUT-NN conversion aims to transform the original weight matrix (depicted as the green matrix) into look-up tables (LUTs) and centroids. The centroids are organized into several codebooks. To achieve this, the


**Figure 2.** LUT-NN-Based Deep Learning Paradigm

**Figure 3.** Computation Reduction Analysis ( $N=H=F=1024$ ).

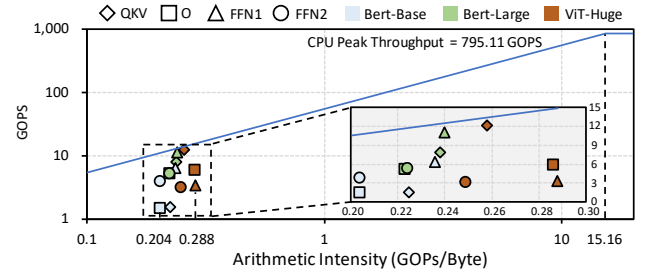
process starts by deriving codebooks through centroid clustering on activation matrices (step ①). Each  $M \times H$  activation matrix, obtained by feeding calibration datasets into a DNN, is divided into  $1 \times V$  sub-vectors along the  $H$  dim, resulting in  $\frac{H}{V}$  columns in total. A codebook is then generated for each column, containing  $CT$  centroids (e.g.,  $CT = 4$  in the figure). Each centroid is a  $1 \times V$  vector, and its values are obtained through K-means clustering of activation sub-vectors within the same column and across activation matrices.

Once the  $\frac{H}{V}$  codebooks are obtained through clustering on the calibration datasets, we proceed to generate the LUTs using the codebooks and weight matrix. The weight matrix with a shape of  $F \times H$  is also split into  $1 \times V$  sub-vectors along the  $H$  dim, and inner-products are performed with the codebooks (step ②). For example, in the figure, the first sub-vectors of the two rightmost codebooks are multiplied with the two rightmost columns in the weight matrix, respectively, which generates the  $F \times 2$  results in the look-up table (step ③). Once all results are generated, it derives  $CT$  look-up tables, each with a shape of  $F \times \frac{H}{V}$ . At this stage, we have successfully converted the  $F \times H$  weight matrix into several LUTs, which can be used in inference together with the codebooks.

### 3.2 LUT-NN Inference

The LUT-NN inference procedure is depicted in Figure 2-(c). When given an input activation matrix with a shape of  $N \times H$ , the conventional GEMM procedure performs matrix multiplication with the  $H \times F$  weight matrix, resulting in a  $N \times F$  output matrix. Here, we demonstrate how an approximated result matrix is obtained using the codebooks and look-up tables derived from the LUT-NN conversion procedure.

Similar to the LUT-NN conversion process, the input activation matrix is divided into several  $1 \times V$  tiles. Each tile is


**Figure 4.** Roofline Analysis of LUT Kernels.

then compared with the codebook of the corresponding column to determine the centroid with the closest L2-distance. This distance estimation is achieved by performing inner-products between the tile and the codebook (Step ④). The index of the best-match centroid is obtained as the argmin value of the inner-product results (Step ⑤). Based on this index, we retrieve a column of data from the indexed look-up table (Step ⑥). For instance, in the figure, if  $argmin = 3$  and the tile corresponds to the right-most column, then the right-most  $F \times 1$  vector is read from  $LT_3$ . These closest-centroid searching and table look-up operations are repeated for each tile (Step ④-⑥). For each row of the activation matrix, the searched  $F \times 1$  vectors are accumulated to generate a column of final results (Step ⑦). After processing all  $N$  rows by repeating ④-⑦, the  $F \times N$  results matrix is formed (Step ⑧).

### 3.3 Affinity Analysis of LUT-NNs on DRAM-PIMs

LUT-NN based inference is suitable for DRAM-PIMs because of two reasons: First, it greatly reduces the computation overhead. For GEMM with the input shape of  $N \times H$  and  $H \times F$ , we need to conduct  $2 \times N \times H \times F$  operations, half of which are multiply operations. For LUT-NN inference with  $CT$  centroids in each codebook and the sub-vector length of  $V$ , we need to conduct  $3 \times N \times H \times CT$  operations for index calculation and  $N \times F \times \frac{H}{V}$  for result accumulation. Specifically, LUT-NN inference only incurs  $N \times H \times CT$  multiplications for index calculation. Considering  $CT$  is much smaller than  $F$ , LUT-NN can greatly reduce the multiplications. In Figure 3, we plot LUT-NN's FLOP count as the bar graphs and use line graphs to illustrate LUT-NN's FLOP reduction



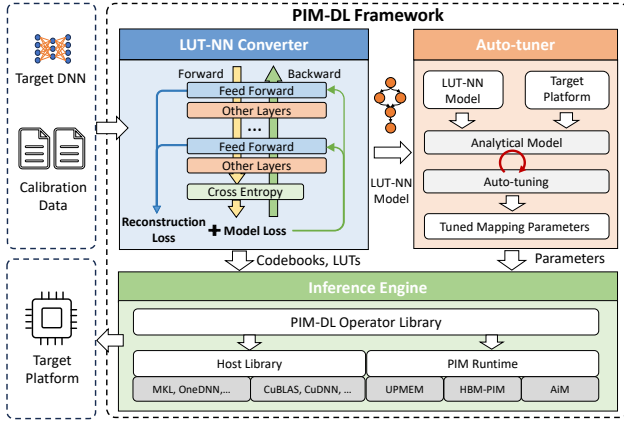


Figure 5. PIM-DL Framework Overview

$(\frac{FLOP_{GEMM}}{FLOP_{LUT-NN}})$ . We can find that LUT-NN greatly reduces computation ( $3.66 \times -18.29 \times$ ) compared with GEMM operations. What's more, multiplications (the green bar) only take up a tiny fraction of LUT-NN's total operations (2.9%-14.3%).

Second, the memory-intensive nature inherent in the LUT-NN inference makes it suitable for DRAM-PIMs. We conduct roofline analysis on LUT-NN based inference to reveal this characteristic. Specifically, we convert the fully-connected (FC) layers in Bert-Base/Large [20] and ViT-Huge [22] to LUT-NN and evaluate their arithmetic intensity on dual-socket Intel Xeon 4210 CPUs by using Intel Advisor tool [40]. We fuse the Q/K/V projection FC layers into one FC operator and quantize all LUTs to INT8 datatype. The inference batch size and sequence length are set to 64 and 512, respectively. As illustrated in Figure 4, we can find that the arithmetic intensity of all operators range from 0.204 to 0.288, all of which fall in the memory-bound region of the CPU.

### 3.4 Challenges of Adopting LUT-NNs

Although LUT-NNs enable the deployment of DNN serving on DRAM-PIMs, we point out that three fundamental challenges hinder their application in practice:

**C1. Unsatisfactory accuracy of the existing LUT-NN conversion algorithm.** The existing LUT-NN conversion algorithm falls short of guaranteeing satisfactory model accuracy. Therefore, [9] only replaces the GEMM in the final classifier layer of DNNs with a lookup table. Although [84] improves upon earlier works, it could still not replace every linear operator. Specifically, [84] could only substitute GEMM in 6 out of the 12 layers of the BERT-base model. If we aim to replace all layers with LUTs, the model's accuracy will become unacceptably low for production environments.

**C2. Existing DL frameworks do not support DRAM-PIMs as the backend.** To deploy converted LUT-NN models on DRAM-PIMs, a deep-learning serving framework that supports both CPU/GPUs and DRAM-PIMs as the backend is necessary. The framework is expected to offload PIM-friendly

operations, especially table lookups to PIMs and the others to the host processors. However, existing inference frameworks [1, 30, 44, 73, 76] do not support commodity DRAM-PIMs, e.g., UPMEM's PIM-DIMM, as the backend.

**C3. Tuning the performance of LUT-NNs on DRAM-PIMs is challenging.** While LUT-NNs offer promising benefits of reduced computation, how to translate such an advantage into real speedup on DRAM-PIMs is still challenging. This difficulty arises due to the architectural limitations present in existing DRAM-PIMs, such as constrained host-PIM communication and inter-PE communication [33]. As a result, processing LUT-NNs on commodity DRAM-PIMs may yield unsatisfactory performance without taking both algorithm and hardware characters into consideration and properly optimizing the hardware mapping.

To overcome these challenges, we propose the PIM-DL framework, which is introduced in the following sections.

## 4 PIM-DL Framework

### 4.1 Framework Overview

Figure 5 outlines the software stack of PIM-DL. To overcome C1, we propose a novel LUT-NN Converter featured with an enhanced LUT-NN calibration algorithm named eLUT-NN. Compared to original LUT-NNs, eLUT-NN is able to replace all linear layers in DNNs with LUTs and maintains high accuracy. To overcome C2, we develop an Inference Engine which implements LUT-NN operators based on host and PIM libraries. To overcome C3, we propose an Auto-Tuner, which analyses the shapes of LUT-NN model and generates the optimized LUT-NN mapping parameters on target hardware platforms. The tuned mapping parameters are fed into the inference engine for efficient LUT-NN serving.

### 4.2 LUT-NN Converter

The LUT-NN Converter is used to convert a trained DNN model into LUT-NN by jointly calibrating the centroids and DNN weights with calibration datasets. As introduced in Section 3, LUT-NN's clustering-based codebook generation may result in approximation errors. Consequently, the previous method [84] can only replace half of the feed-forward layers to maintain accuracy. To deal with this dilemma, we propose a calibration algorithm named eLUT-NN (enhanced LUT-NN) that can correct the error with minor parameter updates. eLUT-NN introduces two new techniques for model calibration: Reconstruction Loss for computation approximation and Straight Through Estimator for gradient propagation.

**Reconstruction Loss for computation approximation:** As illustrated in Figure 5, the reconstruction loss accumulates the errors in all replaced layers and constructs LUT-NN's calibration loss  $L$  together with the original model loss:

$$L = \text{Model Loss} + \beta \sum_{l \in L} \|\hat{A}_l W - A_l W\|^2 \quad (1)$$

In Equation (1),  $A$  represents the original activation matrix, and  $\hat{A}$  denotes the approximated matrix by replacing sub-vectors with the nearest centroids, i.e.,  $\hat{A}_l = H(A_l)$ . Here we use the function  $H(\cdot)$  to denote the closest-centroid-replacing operation. We define the computation error as L2 distance to ensure the reconstruction loss's differentiability, and add a penalty term  $\beta$  to balance the two loss terms.

The reconstruction loss improves model accuracy and facilitates convergence in two main folds. First, it enables direct gradient propagation. Unlike previous work [84] that updates centroids through layer-by-layer back-propagation, the reconstruction loss directly derives the centroid gradients. This approach can overcome the gradient vanishing problem, allowing for direct gradient updates to the centroids. Second, introducing computation errors to the loss function enables the centroids to learn accurate representations of activations, thus accelerating model's convergence.

**Straight Through Estimator for gradient propagation:** Since the centroid clustering and table-lookup operators in LUT-NN conversion are not continuously differentiable, we use the Straight Through Estimator (STE) [93] to estimate the gradients and enable back-propagation. Specifically, to differentiate through the closest-centroid-replacing function  $H(\cdot)$  and pass the error to a function  $F$  that generates the inputs of a layer, we have the following chain rule:

$$\frac{\partial L}{\partial F} = \frac{\partial L}{\partial \hat{y}} \cdot \frac{\partial \hat{y}}{\partial \hat{A}} \cdot \frac{\partial \hat{A}}{\partial A} \cdot \frac{\partial A}{\partial F} \stackrel{\text{STE}}{\approx} \frac{\partial L}{\partial \hat{y}} \cdot \frac{\partial \hat{y}}{\partial \hat{A}} \cdot \frac{\partial A}{\partial F} \quad (2)$$

Where  $\hat{y} = \hat{A} \cdot W$  represents the approximated output of the layer. The STE algorithm assigns  $\frac{\partial \hat{A}}{\partial A}$  to identity to pass through the gradients and enable back-propagation. Compared to the Gumbel-Softmax based gradient-estimation used in previous work [84], our STE-based method ensures faster model convergence according to our experiments.

Comprehensive evaluation results in Section 6 will demonstrate eLUT-NN's two advantages over the baseline method: **A1. High data efficiency.** Unlike the baseline method [84], which demands 100% training set for model calibration, eLUT-NN only requires less than 1% of the pre-training dataset for calibration, and the model converges more quickly.

**A2. High model accuracy.** With the proposed eLUT-NN algorithm, the LUT-NN converter can replace all feed-forward layers of DNNs with LUTs with substantially higher accuracy than the baseline LUT-NN method.

### 4.3 PIM-DL Engine

As depicted in Figure 6-(a), PIM-DL engine comprises a frontend framework and a backend library. The frontend framework encompasses both host and PIM operators, which cover various operators required by LUT-NNs. The host operators are implemented with high-performance tensor libraries on CPUs/GPUs [30, 41, 42, 69, 70]. The PIM operators contain two components: (1) The PIM kernel on the host triggers

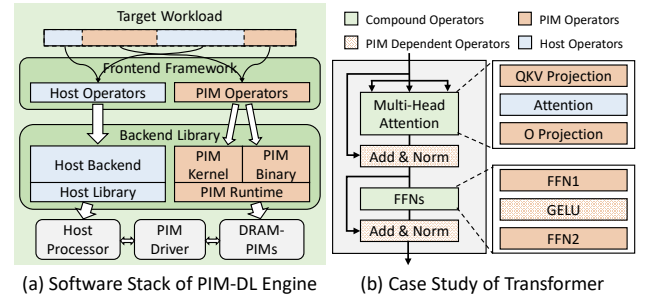


Figure 6. PIM-DL Engine and a Case Study on Transformer.

PIM modules to execute workloads. (2) The PIM binary on the PIM modules describes the offloaded workload. Both host and PIM operators collaborate to implement the LUT-NN's functions. The host processor also controls the PIM binaries' execution via the PIM driver.

Considering transformer has become the de-facto approach in both the neural language processing (NLP) area [11, 20, 64, 78, 79, 92] and the computer vision (CV) area [12, 22, 45, 65, 89, 95], PIM-DL currently mainly focuses on the optimization of transformer-based models. As illustrated in Figure 6-(b), among the basic operators in Transformer [87] models, the QKV projection, Output (O) projection, FFN1, and FFN2 are linear layers. They can be converted to LUTs and offloaded to PIM modules. The attention operator is executed on the host operator, since it cannot be converted to LUTs but requires GEMM operations. The other operators like Add, Norm, GeLU are PIM-friendly element-wise operators. Their offloading choices depend on the functionality supported by target PIM modules.

## 5 Hardware Mapping and Optimization

As analyzed in Section 3.4, considering several architectural limitations of DRAM-PIMs, it is still challenging to efficiently deploy LUT-NNs on DRAM-PIMs. To optimize LUT-NN kernels on different hardware platforms, we design the LUT-NN's mapping strategy and propose the PIM-DL Auto-Tuner, which can generate the best mapping parameters according to the input LUT-NN and the target hardware platform.

In this section, we first present an architecture abstraction of commodity DRAM-PIM products. Subsequently, we delve into a detailed analysis of LUT-NN's mapping on the PIM architecture. Based on this analysis, we model the two essential steps involved in PIM-based LUT-NN operations. We then integrate these steps to establish the PIM-DL Auto-Tuner.

### 5.1 Abstraction of Commodity DRAM-PIMs

As depicted in Figure 7, a DRAM-PIM system is usually composed of a host processor (e.g., CPU, GPU, FPGA) and multiple PIM modules, which are connected to the host's memory channels. In each PIM module, there are distributed computation nodes, which share the same external data bus. Each

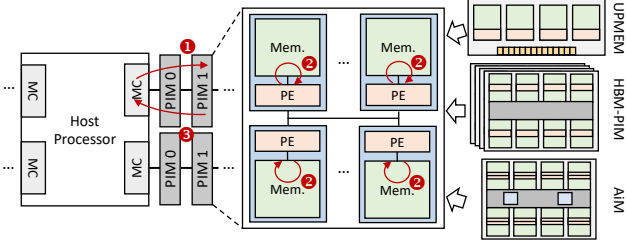


Figure 7. Architecture Abstraction of DRAM-PIM Products.

node contains a Processing Engine (PE) and local memory banks. The PE can be either a general CPU core [18] or a specialized computation engine [54, 55], and may also contain on-chip buffers or registers. Since PEs can conduct memory access concurrently, DRAM-PIMs can provide much higher bandwidth than compute-centric architectures.

Existing commodity DRAM-PIMs adopt the *offloading-based execution model*, i.e., operators in workloads are implemented as PIM kernels, which are offloaded to PIMs for execution. As notated in Figure 7, there are three steps to drive the PIM modules to execute the target workload: ❶ The host processor prepares the input data and sends them to the PIM modules. ❷ After input preparation, the host launches the PIM kernel, which can be either a chunk of codes implemented in PIM’s ISA [18] or a sequence of specified memory commands [55]. ❸ After all PEs finish kernel execution, the host fetches the results from PIM modules. It is worth noting that when deploying applications on DRAM-PIMs, we should consider the following architectural limitations:

**L1: Constrained Host-PIM communication.** As shown in Figure 7, in each PIM module, the PEs collectively share a common memory bus. For example, in UPMEM’s PIM-DIMM architecture, each PE can access only an 8-bit data path, and a group of eight PEs in a rank forms a 64-bit data path. Consequently, the host must transfer data to all PEs in a rank simultaneously to fully utilize the bandwidth. Additionally, it has been demonstrated that broadcasting data from the host to PIMs yields the highest bandwidth, primarily due to the avoidance of cache miss at the host side [33].

**L2: No direct inter-PE datapath.** Due to the scarce on-chip routing resources of DRAM-PIMs [19], no datapath is implemented on UPMEM’s PIM-DIMM and HBM-PIM for inter-PE communication. Therefore, PEs rely on host forwarding to exchange data, which involves loading data from one PE to the host’s cache, then storing it to the destination PE. Considering the poor host-PIM communication ability, inter-PE communication can easily become the performance bottleneck [102]. Therefore, we should avoid costly inter-PE communication when implementing kernels on DRAM-PIMs.

**L3: Load-balancing problem.** Considering that the PIM kernels will be distributed and executed in thousands of PEs, the slowest PE determines the finish time. Therefore, efficient

Table 2. Notations Used in PIM-DL Auto-Tuner

Notation	Description
$N$	Input index’s row count
$CB$	Codebook number ( $CB = \frac{H}{V}$ )
$CT$	Centroid number
$F$	Output feature length
$X_{s-tile}$	Tiling factor of $X$ in sub-LUT partition
$X_{m-tile}$	Tiling factor of $X$ in micro kernel
$X_{load-tile}$	Load factor of $X$ in non-static load schemes
$BW_x^{host}$	Host-PIM bandwidth when transferring tensor $x$
$BW_x^{pim}$	Local memory bandwidth when transferring tensor $x$
$\#PE$	PE number used during execution
$STileSize_x$	Sub-LUT tile size of tensor $x$ transferred to each PE
$MTileSize_x$	On-chip tile size of tensor $x$ during kernel execution
$LCOUNT_x$	Load count of tensor $x$ during kernel execution
$SCOUNT_x$	Store count of tensor $x$ during kernel execution
$RCOUNT$	Reduce count during kernel execution

load balancing is crucial to minimize the overall execution latency and improve resource utilization.

## 5.2 LUT-NN’s Inference Dataflow on DRAM-PIMs

As introduced in Section 3.2, LUT-NN’s inference involves two operators: (1) The *closest centroid search (CCS) operator* (❹-❺ in Figure 2). It computes the distance between the activation matrix and the centroids, then searches the centroids with the shortest distance to generate the index matrix. (2) The *table lookup (LUT) operator* (❻-❼ in Figure 2). It retrieves the lookup table and accumulates the fetched data to derive output results. As illustrated in Figure 8-(a), when executing LUT-NN on DRAM-PIMs, we offload the LUT operator to PIM modules and assign the CCS operator to the host. We avoid processing CCS on PIM since CCS operators are implemented via GEMM and not suitable for DRAM-PIMs.

Another key problem is how to distribute the LUT tasks to thousands of DRAM-PIM PEs to fully utilize the system’s PIM bandwidth. There are two steps to execute LUT on PIM architectures: Step-1: split the workload into sub-LUT workloads, and send each sub-LUT workload to the corresponding PE. Step-2: launch the microkernel on each PE to compute the sub-LUT workloads concurrently. In the following subsections, we will analyze the two steps first. For each step, we will elaborate on the detailed execution dataflow and propose the performance model used for PIM-DL Auto-Tuner. Then, we will put them together to construct the complete design space of LUT-NN inference. The auto-tuner’s workflow is finally introduced to search the optimal parameters. To facilitate understanding, we list the notations used in the following sub-sections in Table 2. In these notations,  $N, CB, CT, F$  specifies the LUT operator’s workload shape.  $X_{s-tile}, X_{m-tile}, X_{load-tile}$  are the tiling factors of each tensor.  $BW_x^{host}, BW_x^{pim}, \#PE$  are parameters related to the underlying DRAM-PIM architecture. The other factors indicate the



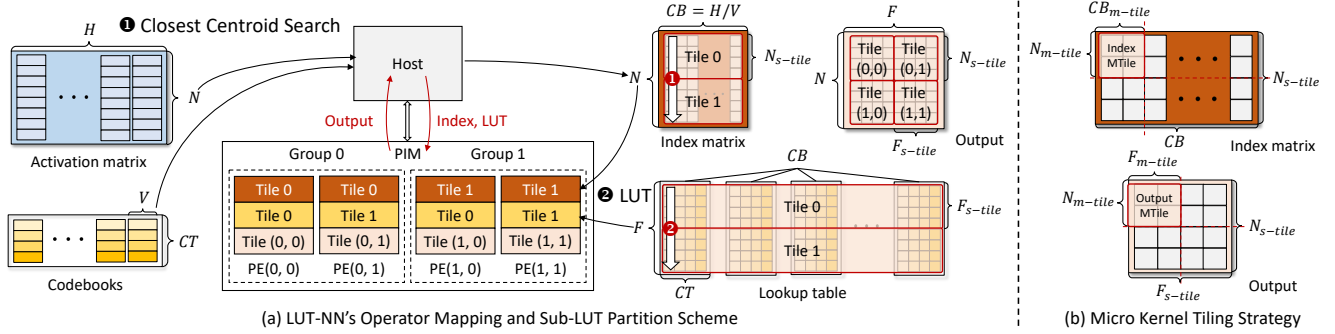


**Figure 8.** Overview of LUT-NN's Execution Dataflow.

tile sizes or operation counts, which can be deduced from the aforementioned parameters.

**5.2.1 Step-1: Sub-LUT Partition.** According to the PIM architecture abstraction discussed in Section 5.1, we propose the sub-LUT partition scheme as illustrated in Figure 8-(a). In this scheme, the index matrix (outputs of the host-side CCS operation, i.e., ❶ in Figure 2) and the LUTs are evenly divided along the index row dim ( $N$ ) and the feature dim ( $F$ ), respectively, while the other dims remain untiled. In addition, the PIM PEs are logically distributed into multiple groups. PEs in the  $i$ -th PE group are responsible for calculating the results of the  $i$ -th index tile. The  $j$ -th PE in each group is responsible for conducting table lookups between its index tile and the  $j$ -th LUT tile. Note that in Figure 8-(a), we use  $CB$  to denote  $\frac{H}{V}$  and transpose the  $CT$  and  $CB$  dims because each index fetches one of the  $CT$  pre-computed results.

Such a partition scheme effectively avoids the limitations discussed above. **For L1:** On the one hand, PEs in the same group share the same index tile, and the  $j$ -th PEs in all groups share the same LUT tile. Tile reuse can enhance the host-PIM communication bandwidth owing to its temporal locality. On the other hand, the codebook dim ( $CB$ ) is not split among PEs, thus ensuring PEs to compute complete results of distinct output tiles and avoiding the extra overhead of partial sum reading and merging. **For L2:** The centroid dim ( $CT$ ) is not split among PEs, so that no inter-PE communication is required when retrieving the LUTs according to the indices. **For L3:** Tiling tensors evenly ensures that each PE's workload size is identical. Since all PEs execute the same micro kernel, we can ensure the load balance among them.

In the example depicted in Figure 8-(a), we use four PEs in total, which are evenly split into two groups. Accordingly, ❶ the index matrix is split into two tiles ( $N = 8$ , and  $N_{s-tile} = 4$ ), and the  $i$ -th tile is broadcast to all PEs in the  $i$ -th PE group ( $i = 0, 1$ ). ❷ The LUT is split into two tiles ( $F = 8$ , and  $F_{s-tile} = 4$ ), and the  $j$ -th tile is broadcast to the  $j$ -th PE in each group ( $j = 0, 1$ ). There are four output tiles, and the  $j$ -th PE in the  $i$ -th group computes output tile  $(i, j)$ 's results.

**Analytical Model:** After sub-LUT partition, we need to send the index tiles and the LUT tiles to each PE before launching the micro kernel. After PEs finishing execution, we need to fetch the output results from them. The host-PIM communication dominates the processing cycles. Therefore, assuming the latency of input sending, LUT sending, and output fetching during the sub-LUT partition stage are denoted as  $t_{index}^{sub}$ ,  $t_{lut}^{sub}$ ,  $t_{output}^{sub}$ , respectively, the sub-LUT partition overhead ( $t_{sub-lut}$ ) can be estimated as:

$$t_{sub-lut} = t_{index}^{sub} + t_{lut}^{sub} + t_{output}^{sub} \quad (3)$$

In Equation (3),  $t_{index}^{sub}$ ,  $t_{lut}^{sub}$ , and  $t_{output}^{sub}$  can be estimated using the transfer size and the bandwidth. Since the transfer pattern affects the bandwidth [33], we use different notations to represent such divergence:

$$t_x^{sub} = \frac{STileSize_x \times \#PE}{BW_x^{host}}, x \in \{index, lut, output\} \quad (4)$$

Note that according to the partition scheme, each PE group holds a index matrix's tile, and each PE in a group is assigned with a LUT table's tile. Therefore, tiling factors in sub-LUT partition should follow the constraint:

$$\#PE = \frac{N}{N_{s-tile}} \times \frac{F}{F_{s-tile}} \quad (5)$$

**5.2.2 Step-2: Micro Kernel Execution.** After sub-LUT partition, the tile size of index matrix, lookup table, and output result in each PE are  $(N_{s-tile}, CB)$ ,  $(CB, CT, F_{s-tile})$ , and  $(N_{s-tile}, F_{s-tile})$ , respectively. To fully utilize PIM PE's on-chip data buffer (e.g. 64KB on each PE in UPMEM PIM-DIMM), we need to further tile these tensors. As illustrated in Figure 8-(b), we conduct tiling along  $(N_{s-tile}, F_{s-tile}, CB)$  dims with tiling factors  $(N_{m-tile}, F_{m-tile}, CB_{m-tile})$ , respectively. In this example, all tiling factors are set to 2. The PIM PE loads one index micro kernel tile (MTile) and the corresponding output MTile each time, then retrieves the LUTs to compute results. For each output MTile, we need to traverse all index MTiles in the same  $N_{m-tile}$ , so that we can reduce data in all codebooks to get the complete results.

**Analytical Model:** The micro kernel's latency ( $t_{micro-kernel}$ ) is the sum of memory transfer latency ( $t_{transfer}$ ) and the LUT



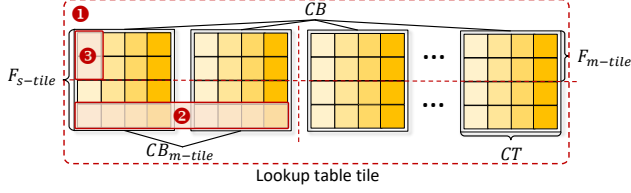


Figure 9. Illustration of LUT Load Schemes.

reduce latency ( $t_{reduce}$ ):

$$t_{micro-kernel} = t_{transfer} + t_{reduce} \quad (6)$$

The memory transfer latency ( $t_{transfer}$ ) is the sum of index load latency ( $t_{index}^{ld}$ ), LUT table load latency ( $t_{lut}^{ld}$ ), and the output result load-store latency ( $t_{output}^{ld}, t_{output}^{st}$ ):

$$t_{transfer} = t_{index}^{ld} + t_{lut}^{ld} + t_{output}^{ld} + t_{output}^{st} \quad (7)$$

We can profile the load/store latency of single tile first, and then use the load/store count induced from the tile traversal order to estimate the total latency:

$$t_x^{ld} = \frac{LCount_x \times MTileSize_x}{BW_x^{pim}}, x \in \{input, lut, output\} \quad (8)$$

$$t_x^{st} = \frac{SCount_x \times MTileSize_x}{BW_x^{pim}}, x \in \{output\} \quad (9)$$

Similarly, we can profile the latency of single reduce ( $t_{single-reduce}$ ) and use the total reduce count to estimate the total reduce latency.  $t_{single-reduce}$  also changes with the underlying DRAM-PIM architecture.

$$t_{reduce} = RCount \times t_{single-reduce} \quad (10)$$

### 5.3 PIM-DL Auto-Tuner

**Search Space.** PIM-DL auto-tuner utilizes four types of mapping parameters involved in LUT-NN's inference dataflow discussed above to construct the search space:

**P1. Sub-LUT Tiling Factors:** The tiling factors, namely  $(N_{s-tile}, F_{s-tile})$ , not only affect the tile sizes assigned to each PE, but also have influence on the communication pattern (i.e. PE group partition) of each tensor. We can exploit these trade-offs by searching different sub-LUT tiling factors.

**P2. Micro Kernel Tiling Factors:** The tile sizes of index MTile and output MTile are  $(N_{m-tile}, CB_{m-tile})$  and  $(N_{m-tile}, F_{m-tile})$ . We can adjust  $(N_{m-tile}, F_{m-tile}, CB_{m-tile})$  to find the optimal buffer allocation between the two MTiles.

**P3. Tile Traversal Order:** Permuting the traversal order of the MTile factors  $(N_{m-tile}, F_{m-tile}, CB_{m-tile})$  changes the sequence of tile delivery, thus affecting the tile reuse pattern [74]. To exploit the effect of different reuse patterns, we add the tile traversal order to the search space.

**P4. LUT load scheme:** Since the LUT's elements are fetched according to the input index, we can either load the LUT in bulk or on-demand. We include three LUT load schemes into our design space, which are illustrated in Figure 9:

### Algorithm 1: Auto-tuning Workflow

```

1 Input: Workload Size  $(N, CB, CT, F)$ 
2  $Cost = MaxValue$ 
3  $MappingParams = \{\}$ 
4 for each legal  $(N_{s-tile}, F_{s-tile})$  do
5     // estimate sub-LUT partition overhead
6      $t_{sub-lut} = t_{index}^{sub} + t_{lut}^{sub} + t_{output}^{sub}$ 
7     // search for the optimal micro-kernel
8      $t_{micro-kernel}^*, Kernel^* =$ 
9      $KernelSearch(N_{s-tile}, F_{s-tile}, CB, CT)$ 
10    // update the optimal parameters
11    if  $t_{sub-lut} + t_{micro-kernel}^* < Cost$  then
12         $Cost = t_{sub-lut} + t_{micro-kernel}^*$ 
13         $MappingParams = \{N_{s-tile}, F_{s-tile}, Kernel^*\}$ 
13 return  $Cost, MappingParams$ 

```

1. **Static Load.** When each PE's LUT MTile size is smaller than the on-chip buffer size, we can place the whole LUT on-chip statically. In this way, we can load the LUT once and reuse it during the execution. We need to hold  $CB_{s-tile} \times CT \times F_{s-tile}$  LUT elements in the on-chip buffer.

2. **Coarse-grain Load.** Since each index selects the target element from every  $CT$  candidates, we can load these  $CT$  elements to the on-chip buffer and reuse them. In this way, we load  $CB_{load-tile} \times CT \times F_{load-tile}$  elements in the LUT each time. In Figure 9, we set  $CB_{load-tile} = 2$  and  $F_{load-tile} = 1$  for coarse-grain load scheme. These elements will be buffered till the corresponding codebooks have been reduced.

3. **Fine-grain Load.** We can also load the LUT's elements on-demand. In this way, we load  $F_{load-tile}$  LUT values along the feature dim when we process a new index. In Figure 9, we set  $F_{load-tile} = 2$  for fine-grain load scheme. Specifically, if the PE can issue multiple read requests in parallel, we will hold  $F_{load-tile}$  LUT elements for each parallel slot. For example, UPMEM's PE contains multiple hardware threads [18], each of which can issue independent memory requests. Therefore, we keep a buffer with  $F_{load-tile}$  LUT elements for each activated hardware thread.

Among these parameters, the micro kernel tiling factors, tile traversal order, and LUT load scheme jointly construct the micro kernel's mapping space.

**Auto-Tuning Workflow:** PIM-DL auto-tuner's workflow is listed in Algorithm 1. Given the workload size  $(N, CB, CT, F)$ , PIM-DL auto-tuner traverses all legal sub-LUT tiling factors. For each legal factor pair  $(N_{s-tile}, F_{s-tile})$ , the auto-tuner first calculates  $t_{sub-lut}$ . Then, the auto-tuner searches the micro kernel's mapping space and reports the parameters with the minimum execution latency  $t_{micro-kernel}^*$ . The total execution latency of current sub-LUT tiling strategy is the sum of  $t_{sub-lut}$  and  $t_{micro-kernel}^*$ . By comparing the total execution latency, the auto-tuner generates the most efficient hardware mapping. For a given model, PIM-DL auto-tuner searches for the optimal parameters of all LUT kernels offline. Given

**Table 3.** Configuration of DRAM-PIM Platforms

<b>DDR4-PIM Platform</b>	Host	Xeon 4210 CPU $\times$ 2 128GB DDR4 Memory
	DRAM-PIM	UPMEM PIM-DIMM $\times$ 8 1024 PEs, 64 GB DDR4 Memory
<b>HBM-PIM Platform (Simulated)</b>	Host	NVIDIA A2 GPU $\times$ 1 16 GB GDDR6 Memory
	DRAM-PIM	Samsung HBM-PIM Cube $\times$ 4 512 PEs, 8 GB HBM2 Memory
<b>AiM Platform (Simulated)</b>	Host	NVIDIA A2 GPU $\times$ 1 16 GB GDDR6 Memory
	DRAM-PIM	SK-Hynix AiM Chip $\times$ 16 512 PEs, 16 GB GDDR6 Memory

the input shape, each model need to be tuned only once, which only incurs little overhead ( $\sim$ 1s/model on dual-socket Intel Xeon 4210 CPUs) compared with the latency of model inference (tens of seconds/model on our UPMEM platform).

## 6 Evaluation

### 6.1 Experiment Setup

**Models:** For accuracy validation, we evaluate eLUT-NN on both NLP and CV tasks. Specifically, for NLP tasks, we evaluate the popular BERT-base and BERT-large models [20] on the GLUE [88] benchmark dataset. For CV tasks, we evaluate ViT-base and ViT-huge [22] on the CIFAR-10 and CIFAR-100 [53] datasets. For throughput comparison, since the model size of BERT-base is identical to ViT-base, we evaluate the BERT-base, BERT-large, and the ViT-huge models, whose hidden dim sizes are 768/1024/1280, respectively.

**Platforms:** Our main experiments are conducted on a real DRAM-PIM platform, namely UPMEM PIM-DIMM [18]. The configuration details are presented in Table 3. This platform equips dual-socket Intel Xeon 4210 CPUs. Each socket designates two channels for conventional DDR4 DIMMs and two channels for UPMEM PIM-DIMMs. Each of the 8 PIM-DIMMs contains two ranks, and each rank equips 64 PEs. The host operators are implemented with C++/OpenMP [14] and GGML tensor library [30], which leverages AVX intrinsics to accelerate inference on x86 CPUs. The PIM operators are implemented with the UPMEM SDK [86] (Version 2021.3.0).

Given that Samsung’s HBM-PIM and SK-Hynix’s AiM have not been available yet, our evaluation of PIM-DL on these potential platforms is conducted through simulation. We use the simulator officially released by Samsung [71] and extend it to support AiM’s functionality. An NVIDIA A2 GPU serves as the host for the two PIM products. We implement the host operators with Pytorch [76] and conduct simulations to estimate the PIM operators’ performance.

**Baselines:** We compare eLUT-NN with the baseline LUT-NN [84] in term of accuracy. Both algorithms adopt full-layer replacement. The original model accuracy is obtained from BERT and ViT papers [20, 22]. For throughput evaluation, we compare PIM-DL on DDR4-PIM with GGML [30]-based

**Table 4.** NLP Model Accuracy

Model	Settings	MNLI	QQP	QNLI	SST-2	CoLA	STS-B	MRPC	RTE	Avg.
BERT-base	Original	83.4	71.2	90.5	93.5	52.1	85.8	88.9	66.4	79.0
	LUT-NN	35.5	63.2	50.6	49.3	0.0	1.36	31.6	52.7	35.5
	eLUT-NN	79.9	69.6	87.4	92.4	51.2	83.2	87.1	64.7	76.9
BERT-large	Original	85.9	72.1	92.7	94.9	60.5	86.5	89.3	70.1	81.5
	LUT-NN	34.7	62.7	51.3	52.2	0.0	4.40	38.7	50.5	36.8
	eLUT-NN	82.1	71.0	90.2	93.1	56.8	86.7	86.1	68.4	79.3

**Table 5.** Vision Model Accuracy

Model	Settings	CIFAR-10	CIFAR-100	Model	Settings	CIFAR-10	CIFAR-100
ViT-base	Original	98.5	91.4	ViT-huge	Original	99.5	94.55
	LUT-NN	10.1	1.07		LUT-NN	10.0	1.01
	eLUT-NN	96.3	89.1		eLUT-NN	97.8	91.32

transformer inference on a CPU server which equips dual-socket Intel Xeon Gold 5218 CPUs (8 channels, 512 GB DDR4 memory). The baselines adopt FP32/INT8 datatype, and the INT8 baselines are optimized with AVX/AVX2 intrinsics in GGML. We compare the HBM-PIM/AiM based PIM-DL with a DGX-1 workstation equipping 32GB NVIDIA V100 GPUs. On the DGX station, we implement FP32-based model inference with PyTorch [76]. Besides, we also compare the HBM-PIM/AiM based PIM-DL with GEMM-based inference on these platforms. In these baselines, we offload all linear layers to DRAM-PIMs, and implement other GPU-side operators with PyTorch [76]. We adopt FP16 datatype on the HBM-PIM platform and BF16 datatype on the AiM platform. In all baselines, we use the model architectures proposed in Bert/ViT papers [20, 22] without pruning/sparsification.

### 6.2 Model Accuracy

During calibration, all models are initialized using the pre-trained model weights, and the centroids are initialized randomly. We set the sub-vector length and the centroid number to 2 and 16, and set the reconstruction loss penalty term  $\beta$  to  $1e-3$  for BERT models,  $1e-4$  for ViT models. The learning rate is  $1e-5$  for BERT-large and  $5e-5$  for other models. The tokens used in LUT-NN calibration are randomly sampled from the datasets using the dataloader provided by Pytorch.

Table 4 and 5 presents the accuracy results. We can find that even though the original LUT-NN algorithm consumes the whole training set, it still has great accuracy degradation (90.44%/44.10% average drop on CV/NLP tasks) when all linear layers are replaced. eLUT-NN models reach convergence after no more than 100k iterations and consume only  $\sim$ 0.78% of tokens in the training set. Besides, eLUT-NN greatly enhances the accuracy compared with the baseline LUT-NN (88.09%/41.95% average improvement on CV/NLP tasks) and also achieves accuracy close to the original models (2.36%/2.25% average drop on CV/NLP tasks).

### 6.3 End-to-end Performance

**Throughput:** We first compare DDR4-PIM based PIM-DL’s performance against the CPU server. For BERT-base and

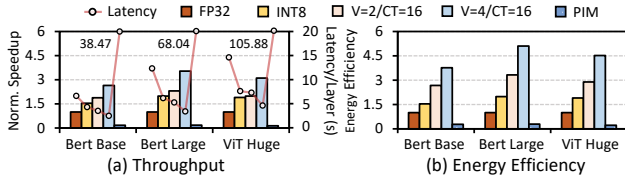


Figure 10. End-to-end performance comparison.

BERT-large, we set the sequence length to 512 and the batch size to 64. For ViT-huge model, we set the shape of an input image to  $224 \times 224 \times 3$ , and the batch size is 128. Under a patch size of  $14 \times 14$ , ViT-huge’s sequence length is 257. We pad the sequence length to 264 to evenly partition the workload among PIM PEs. Considering UPMEM’s low FP32 computation capacity, we conduct INT8 quantization on the LUTs, which reports  $\leq 0.1\%$  accuracy drop. On the CPU server, we evaluate the inference performance with FP32/INT8 data precision. For PIM-DL’s inference, we set  $CT=16$  and  $V=2$  or 4. We also evaluate the performance by offloading all linear layers without LUT-NN conversion.

As Figure 10-(a) shows, we plot the speedup as bar graphs and use line graphs to illustrate the inference latency (recorded in second). Compared with FP32/INT8 inference on CPU server, PIM-DL achieves  $2.05 \times / 1.14 \times$  geomean speedup under the  $V=2/CT=16$  setting and further achieves  $3.07 \times / 1.71 \times$  geomean speedup under the  $V=4/CT=16$  setting. Besides, compared with the model inference performance on PIM architecture, PIM-DL achieves  $12.61 \times / 18.91 \times$  geomean speedup under the two settings, respectively. PIM-DL successfully enables deep learning on UPMEM’s commodity PIM-DIMMs and brings considerable performance improvement.

**Energy Efficiency:** We compare the energy consumption (in Joules) of DDR4-PIM based PIM-DL against the baselines on the CPU server. We adopt Intel RAPL [43] to measure the CPU’s energy. We adopt the power provided by *dpu-diag* tool in UPMEM SDK [86] for PIM-DIMM’s energy estimation, which reports  $\sim 13.92W/DIMM@350MHz$ . It is the static power of both the PIM cores and the PIM banks. Considering PIM-DIMMs do not use dynamic voltage and frequency scaling (DVFS), this static power is close to PIM-DIMM’s dynamic power. Besides, this power is also in alignment with the power officially released by UPMEM [19]. The memory access energy between the CPU and the PIM-DIMMs is measured using the MSR\_DRAM\_ENERGY\_STATUS register provided by Intel RAPL following Intel’s manual [39]. As illustrated in Figure 10-(b), all results are normalized to FP32 CPU baseline. Compared with FP32/INT8 inference on the CPU server, PIM-DL achieves  $2.95 \times / 1.65 \times$  ( $V=2/CT=16$ ) and  $4.42 \times / 2.46 \times$  ( $V=4/CT=16$ ) higher energy efficiency (geomean). Compared with PIM-based original model inference, PIM-DL achieves  $11.16 \times$  ( $V=2/CT=16$ ) and  $16.74 \times$  ( $V=4/CT=16$ ) higher energy efficiency (geomean).

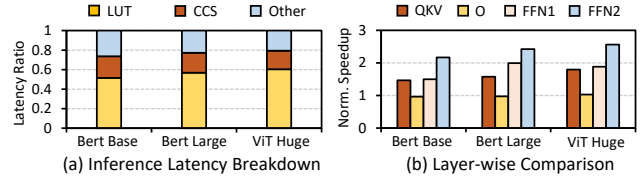


Figure 11. Performance analysis.

## 6.4 Performance Analysis

**Latency Breakdown:** To better understand the performance improvement of PIM-DL, we first breakdown the latency of PIM-DL into LUT operator’s latency, CCS operator’s latency, and other operators’ latency. As depicted in Figure 11-(a), LUT-NN inference takes up  $73.73\% \sim 79.39\%$  of total latency. Specifically, the LUT operator’s latency takes up  $69.88\% \sim 76.10\%$  of LUT-NN inference latency, and thus takes up  $51.52\% \sim 60.41\%$  of total latency. Such results demonstrate that PIM-DL can offload much more portion of deep learning workloads than existing PIM-enabled systems, which considerably improves DRAM-PIM’s utilization.

**Layer-wise Performance Comparison:** We further analyse the speedup of each linear layer with the replacement of LUT-NN. We compare their performance between LUT-NN inference ( $V=4/CT=16$ ) and GEMM-based INT8 inference on the CPU server. As depicted in Figure 11-(b), these layers can bring  $1.81 \times$  geomean speedup in total, and each of them can gain  $1.61 \times$ ,  $0.99 \times$ ,  $1.78 \times$ , and  $2.38 \times$  geomean speedup, respectively. FFN2 gains the highest performance improvement because it has the largest inner dim in GEMM operations. For QKV projection and FFN1, we can also gain better performance because they have large output feature dims. Even for the smallest O projection, PIM-DL’s performance is also comparable to the CPU server’s performance.

## 6.5 Sensitivity Analysis

To explore the scalability of DDR4-PIM based PIM-DL, we conduct sensitivity analysis and change four parameters: sub-vector length ( $V$ ), centroid number ( $CT$ ), batch size, and hidden dim. By default, we set  $V=4$ ,  $CT=16$ , sequence length to 512, and batch size to 64 for all models. All results are normalized to CPU server’s INT8 inference performance.

**Sub-vector Length:** As depicted in Figure 12-(a), when the sub-vector length is larger, we can gain better performance because larger sub-vector length decreases codebook number, thus shrinking the LUTs’ size. However, the performance improvement tends to coverage because UPMEM product’s bandwidth decreases when transfer size shrinks [33].

**Centroid Number:** In Figure 12-(b), we can find that when centroid number shrinks, we can gain better performance because the LUTs’ memory footprints decrease. Similar to sub-vector length, the performance improvement has slight tendency to converge with centroid number decreasing.



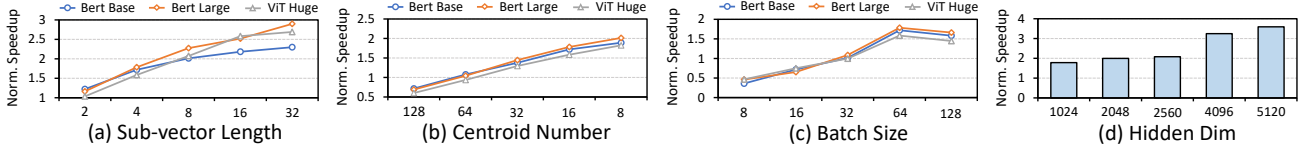


Figure 12. Sensitivity analysis of different parameters.

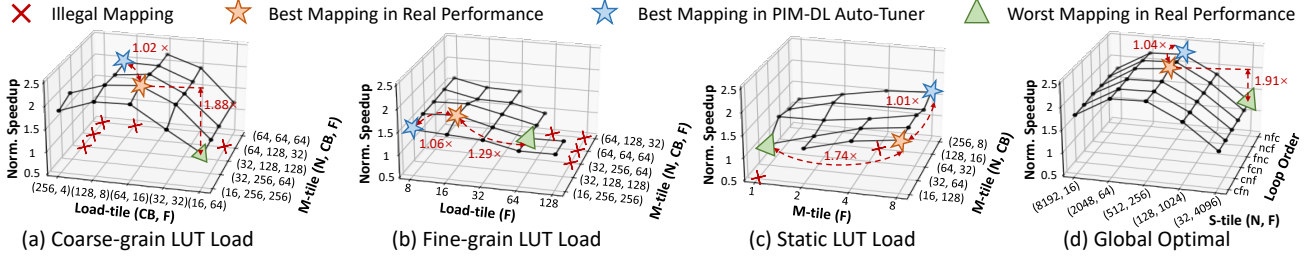


Figure 13. Illustration of LUT-NN inference's mapping space.

**Batch Size:** As Figure 12-(c) shows, when the batch size is small, the CPU server outperforms PIM-DL. That is because when executing small kernels on UPMEM PIM-DIMMs, the poor host-PIM communication bandwidth becomes the main bottleneck [31, 33, 48]. When the PIM kernel becomes larger, such issue will be alleviated.

**Hidden Dim:** We also exploit the performance when changing the hidden dim size. We select several commonly used hidden dim sizes from [99] and illustrate the results in Figure 12-(d). PIM-DL achieves 2.44× geomean speedup against the CPU server. Specifically, when the hidden dim size comes to 4096, PIM-DL gains much better performance because CPU server has poorer scalability than PIM-DL.

### 6.6 Mapping Space Visualization

To visualize LUT-NN's mapping space on UPMEM's PIM-DIMM, we take BERT-large's FFN1 layer as a case study. The workload shape  $(N, CB, CT, F)$  is  $(32768, 256, 16, 4096)$ , and we set  $(N_{s-tile}, F_{s-tile})$  to  $(16384, 8)$  for static LUT load scheme, and  $(512, 256)$  for the other LUT load schemes. As shown in Figure 13, we illustrate the neighborhood of the best mapping parameters under three LUT load schemes and depict the global optimal parameters when changing sub-LUT tiling factors and tile traversal order.

**Sub-LUT Tiling Factors:** As depicted in Figure 13-(d), changing  $(N_{s-tile}, F_{s-tile})$  can bring up to 1.91× performance gap. That is because when  $N_{s-tile}$  or  $F_{s-tile}$  is large, the skew of tile size leads to higher host-PIM communication overhead.

**Micro Kernel Tile Size:** For coarse-grain or fine-grain LUT load schemes, the average performance gap brought by changing micro kernel tile sizes is 1.04×. However, for static LUT load scheme, changing micro kernel tile sizes can bring up to 1.74× performance gap. That is because under the static scheme,  $F_{m-tile}$  is bounded by  $F_{s-tile}$ : To hold the LUTs on PE's on-chip buffer, we can only set  $F_{s-tile}$  to at most 8 under

the given workload shape. PE's DRAM bandwidth does not saturate and increases rapidly under such a low  $F_{m-tile}$ .

**Tile Traversal Order:** From Figure 13-(d), we can infer that changing the tile traversal order brings little performance divergence. That is because due to the wimpy computation capacity of PEs in UPMEM's product, the accumulation latency takes up most of the micro kernel's execution latency, which diminishes the benefit of exploiting on-chip data reuse.

**LUT Load Scheme:** As illustrated in Figure 13-(a)-(b), adjusting load tile sizes can bring considerable performance gap. That is because the offsets of on-chip tiles are also computed by the PE. Since the on-chip buffer's bandwidth is related to the instruction number [33], we need to set moderate load tile sizes to fully utilize the on-chip buffer's bandwidth.

**Auto-Tuner Analysis:** As illustrated in Figure 13, the parameters provided by PIM-DL Auto-Tuner bring  $\leq 6\%$  performance degradation. Besides, the average error of performance estimation is 3.44%, and the max error is 13.73%. The PIM-DL auto-tuner can help us to automatically find a near-optimal parameter for given workloads.

### 6.7 PIM-DL on HBM-PIM and AiM

Apart from UPMEM PIM-DIMM, we also evaluate PIM-DL on HBM-PIM/AiM products via simulation. We set the transformer's sequence length to 128, and adjust the batch size from 1 to 8. The hidden dims are selected from [99]. We assume PIM instructions carry the LUT indices and drive the execution of PEs during PIM-DL's inference.

We first compare the performance between PIM-DL and the normal DNN inference on the two products. As depicted in Figure 14, PIM-DL achieves 23.94×/19.06× geomean speedup on HBM-PIM/AiM, respectively. When the batch size increases, PIM-DL's performance gain increases by up to 2.23×, because larger batch sizes are unfriendly to the two products. On the other hand, when the hidden dim increases,

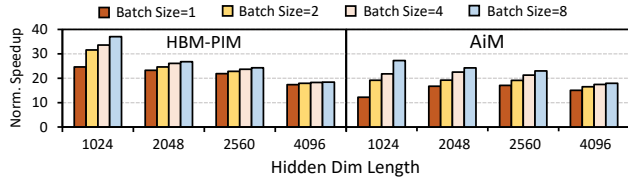


Figure 14. Normal PIM-based DNN inference VS. PIM-DL.

the speedup of PIM-DL against the baselines slightly shrinks. This is because HBM-PIM and AiM’s dataflow is optimized for processing matrices with flat shapes.

We also compare PIM-DL on the two products with a V100 GPU baseline running FP32 models. As illustrated in Figure 15, AiM-based PIM-DL outperform NVIDIA V100 GPU by up to 1.20×, while HBM-PIM-based PIM-DL can only achieve 39% of V100’s performance (geomean). That is because the huge computation capacity gap between V100 GPU (130 TFLOPS) and HBM-PIM (4.8 TFLOPS). For AiM, since the computation capacity is much higher than HBM-PIM (16 TFLOPS), PIM-DL can provide comparable performance against inference on the V100 GPU.

## 7 Discussion and Future Work

Finally, we list some architecture implications which can further improve PIM-DL’s performance on DRAM-PIMs.

**Adder-only PIM Design:** As discussed in Section 3.3, LUT-NN removes all multiplications in the PIM-side LUT operators. Therefore, we can equip adder-only PEs in DRAM-PIMs. Considering adders have much lower hardware overhead than multipliers [46], we can equip much more adders under the same area/power constraints. PIM-DL on such adder-only DRAM-PIMs will achieve much higher performance.

**On-chip Buffer Management Support:** PIM-PE’s on-chip buffer cannot support to exploit data reuse because of the severe overhead to implement caching mechanism [85]. Therefore, we only adopt three simple LUT load schemes Since the LUT access depends on the distribution of centroid indices, which may skew to several "hot" items, exploiting data reuse with better support of on-chip buffer management can bring better performance to PIM-DL.

## 8 Related Work

DRAM-PIMs have been proposed for many years to address the "Memory-Wall" problem. Many academic proposals utilize DRAM-PIMs to accelerate data-intensive applications in scenarios like graph processing [2, 15, 67, 97, 104], machine learning [3, 28, 37, 50, 52, 56, 60, 61, 63, 75, 80, 90, 94, 101], and general-purpose applications [4, 10, 25, 27, 32, 35, 38, 91, 96]. They can be categorized into two major types: (1) DRAM-PIMs built with die-stacking memories, e.g., Hybrid Memory Cube (HMC). For example, GraphP [98] and GraphQ [104] adopts HMC to accelerate graph processing. SynCron [32]

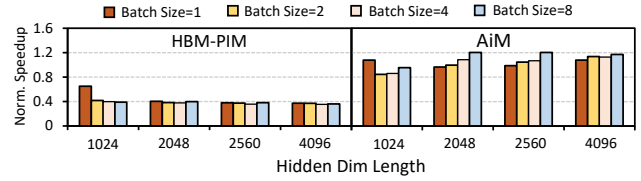


Figure 15. GPU-based inference VS. PIM-DL.

proposes efficient synchronization support on HMC for data intensive applications. (2) DRAM-PIMs built with Dual-Inline Memory Modules (DIMMs). For example, TensorDIMM [57] and RecNMP [51] accelerate recommendation systems with near-memory tensor reduction. DIMM-Link [102] presents a full-stack design to enhance the inter-DIMM communication performance for generic DIMM-NMP architectures.

In recent few years, DRAM-PIMs have entered the commercialization phase. UPMEM has proposed PIM-DIMM [18], which equips RISC cores near DRAM banks. Samsung and SK-Hynix have introduced HBM-PIM [55]/AiM [54] to accelerate memory-bound operators in deep learning applications. Although there are various proposals customizing real-world applications on commodity DRAM-PIMs [6–8, 16, 21, 31, 34, 48, 49, 58, 62, 72], none of them can efficiently process mainstream DNNs such as transformers. To our best knowledge, PIM-DL is the first full-stack framework that expands DRAM-PIMs’ applicability under deep learning scenarios. Unlike previous proposals implementing LUT-based operations in DRAM circuits [17, 26, 82, 83, 100], we adopt LUTs in the algorithm level, ensuring PIM-DL’s efficient deployment on real-world DRAM-PIM products. Although TransPimLib [72] implements LUT-based transcendental functions on UPMEM PIM-DIMMs, it cannot be directly used to accelerate GEMM. PIM-DL and provides algorithmic innovation to maintain the model accuracy when substituting GEMM to LUT-NN and contains efficient mapping & auto-tuning strategies to boost the performance of model inference.

## 9 Conclusion

This paper proposes PIM-DL, the first full-stack framework to expand the applicability of commodity DRAM-PIMs for deep learning. We adopt the eLUT-NN algorithm for model calibration and design the PIM-based inference backend, including the PIM-DL Engine and the Auto-Tuner. Compared with GEMM-based inference on DRAM-PIMs, PIM-DL achieves 22.6×~37.1× speedup. Compared with inference on CPU/GPU, PIM-DL achieves up to 3.54×/1.20× speedup.

## Acknowledgments

We thank all the reviewers and our shepherd for their valuable comments. We also thank Yiqi Chen for his help on proof reading. This work is supported by NSF China (62032001) and 111 Project (B18001).

## A Artifact Appendix

### A.1 Abstract

This artifact contains the source code of PIM-DL, including the implementation of model calibration, auto-tuner, and the inference engine. In addition, this artifact provides config files and scripts to reproduce the key experimental results reported in the paper.

### A.2 Artifact check-list (meta-information)

- **Algorithm:** LUT-based neural network (LUT-NN).
- **Program:** Python3, C, C++.
- **Compilation:** The compiler provided in UPMEM SDK (Version 2021.3.0), which is based on clang 10.0.0.
- **Run-time environment:** The system is developed and tested in Ubuntu 18.04.6 LTS (GNU/Linux 4.15.0-184-generic x86\_64).
- **Hardware:** The experiments were run on a machine with Intel Xeon 4210 CPU (dual-socket), 128 GB memory, and 8 UPMEM PIM-DIMMs (8GB/DIMM, DPU running at 350 MHz).
- **Execution:** Make sure no other workloads are running on the system during the experiment.
- **Metrics:** Normalized speedup and energy efficiency.
- **Output:** The resulting figures shown in paper for key experiments.
- **Experiments:** Scripts are included in the `asplos24-ae` folder. Detailed instructions are provided in `asplos24-ae/README.md`.
- **How much disk space required (approximately)?:** About 1GB.
- **How much time is needed to prepare workflow (approximately)?:** About 10 minutes.
- **How much time is needed to complete experiments (approximately)?:** About 3 hours.
- **Publicly available?:** Yes. Github link: <https://github.com/leesou/PIM-DL-ASPLOS>.
- **Code licenses (if publicly available)?:** MIT License.
- **Archived (provide DOI)?:** Yes. DOI link: <https://doi.org/10.5281/zenodo.10531532>

### A.3 Description

**A.3.1 How to access.** For AE reviewers, considering it might be difficult to prepare a server equipped with UPMEM PIM-DIMMs, we provide ssh access to our server. For others who want to reproduce these experiments, we provide the open-sourced project on Github (Link: <https://github.com/leesou/PIM-DL-ASPLOS>), but the following dependencies should be satisfied.

**A.3.2 Hardware dependencies.** All experiments are run on a machine with Intel Xeon 4210 CPU (dual-socket), 128 GB memory, and 8 UPMEM PIM-DIMMs (8GB/DIMM, DPU running at 350 MHz).

**A.3.3 Software dependencies.** To use UPMEM PIM-DIMMs, UPMEM's SDK toolchain needs to be installed on the server. The SDK version on our server is 2021.3.0. Besides,

our server runs on Ubuntu 18.04.6 LTS (GNU/Linux 4.15.0-184-generic x86\_64).

### A.4 Installation

Installation instructions are provided in the `asplos24-ae` folder. Please check `asplos24-ae/README.md` for more details.

### A.5 Experiment workflow

Experiment scripts are provided in the `asplos24-ae` folder. Please check `asplos24-ae/README.md` for more details.

### A.6 Evaluation and expected results

After finishing execution, all plotted results are saved in the `asplos24-ae/results` folder. These results should be in correspondence with Figure 10, 11, 12, and 13. Note that the results might be slightly different from that in the paper due to the runtime perturbation, but the trends should be similar. Please check `asplos24-ae/README.md` for more information on result validation.

## References

- [1] Martín Abadi, Ashish Agarwal, Paul Barham, Eugene Brevdo, Zhifeng Chen, Craig Citro, Greg S Corrado, Andy Davis, Jeffrey Dean, Matthieu Devin, et al. Tensorflow: Large-scale machine learning on heterogeneous distributed systems. *arXiv preprint arXiv:1603.04467*, 2016.
- [2] Junwhan Ahn, Sungpack Hong, Sungjoo Yoo, Onur Mutlu, and Kiyoung Choi. A scalable processing-in-memory accelerator for parallel graph processing. In *Proceedings of the 42nd Annual International Symposium on Computer Architecture*, pages 105–117, 2015.
- [3] Bahar Asgari, Ramyad Hadidi, Jiashen Cao, Sung-Kyu Lim, Hyesoon Kim, et al. Fafnir: Accelerating sparse gathering by using efficient near-memory intelligent reduction. In *2021 IEEE International Symposium on High-Performance Computer Architecture (HPCA)*, pages 908–920. IEEE, 2021.
- [4] Hadi Asghari-Moghaddam, Young Hoon Son, Jung Ho Ahn, and Nam Sung Kim. Chameleon: Versatile and practical near-dram acceleration architecture for large memory systems. In *2016 49th annual IEEE/ACM international symposium on Microarchitecture (MICRO)*, pages 1–13. IEEE, 2016.
- [5] Jimmy Lei Ba, Jamie Ryan Kiros, and Geoffrey E Hinton. Layer normalization. *arXiv preprint arXiv:1607.06450*, 2016.
- [6] Alexander Baumstark, Muhammad Attahir Jibril, and Kai-Uwe Sattler. Accelerating large table scan using processing-in-memory technology. *BTW 2023*, 2023.
- [7] Alexander Baumstark, Muhammad Attahir Jibril, and Kai-Uwe Sattler. Processing-in-memory for databases: Query processing and data transfer. In *Proceedings of the 19th International Workshop on Data Management on New Hardware*, pages 107–111, 2023.
- [8] Arthur Bernhardt, Andreas Koch, and Iliia Petrov. pimdb: From main-memory dbms to processing-in-memory dbms-engines on intelligent memories. In *Proceedings of the 19th International Workshop on Data Management on New Hardware*, pages 44–52, 2023.
- [9] Davis W. Blalock and John V. Guttag. Multiplying matrices without multiplying. In Marina Meila and Tong Zhang, editors, *Proceedings of the 38th International Conference on Machine Learning, ICML 2021, 18-24 July 2021, Virtual Event*, volume 139 of *Proceedings of Machine Learning Research*, pages 992–1004. PMLR, 2021.



- [10] Amiral Boroumand, Saugata Ghose, Minesh Patel, Hasan Hassan, Brandon Lucia, Rachata Ausavarungnirun, Kevin Hsieh, Nastaran Hajinazar, Krishna T Malladi, Hongzhong Zheng, et al. Conda: Efficient cache coherence support for near-data accelerators. In *Proceedings of the 46th International Symposium on Computer Architecture*, pages 629–642, 2019.
- [11] Tom Brown, Benjamin Mann, Nick Ryder, Melanie Subbiah, Jared D Kaplan, Prafulla Dhariwal, Arvind Neelakantan, Pranav Shyam, Girish Sastry, Amanda Askell, et al. Language models are few-shot learners. *Advances in neural information processing systems*, 33:1877–1901, 2020.
- [12] Nicolas Carion, Francisco Massa, Gabriel Synnaeve, Nicolas Usunier, Alexander Kirillov, and Sergey Zagoruyko. End-to-end object detection with transformers. In *European conference on computer vision*, pages 213–229. Springer, 2020.
- [13] Jason Cong, Zhenman Fang, Michael Gill, Farnoosh Javadi, and Glenn Reinman. AIM: accelerating computational genomics through scalable and noninvasive accelerator-interposed memory. In *Proceedings of the International Symposium on Memory Systems, MEMSYS 2017, Alexandria, VA, USA, October 02 - 05, 2017*, pages 3–14. ACM, 2017.
- [14] Leonardo Dagum and Ramesh Menon. Openmp: an industry standard api for shared-memory programming. *IEEE computational science and engineering*, 5(1):46–55, 1998.
- [15] Guohao Dai, Tianhao Huang, Yuze Chi, Jishen Zhao, Guangyu Sun, Yongpan Liu, Yu Wang, Yuan Xie, and Huazhong Yang. Graphh: A processing-in-memory architecture for large-scale graph processing. *IEEE Transactions on Computer-Aided Design of Integrated Circuits and Systems*, 38(4):640–653, 2018.
- [16] Prangon Das, Purab Ranjan Sutradhar, Mark Indovina, Sai Manoj Pudukotai Dinakarrao, and Amlan Ganguly. Implementation and evaluation of deep neural networks in commercially available processing in memory hardware. In *2022 IEEE 35th International System-on-Chip Conference (SOCC)*, pages 1–6, 2022.
- [17] Quan Deng, Youtao Zhang, Minxuan Zhang, and Jun Yang. Lacc: Exploiting lookup table-based fast and accurate vector multiplication in dram-based cnn accelerator. In *Proceedings of the 56th Annual Design Automation Conference 2019*, pages 1–6, 2019.
- [18] Fabrice Devaux. The true processing in memory accelerator. In *2019 IEEE Hot Chips 31 Symposium (HCS)*, pages 1–24. IEEE Computer Society, 2019.
- [19] Fabrice Devaux. The true processing in memory accelerator. In *2019 IEEE Hot Chips 31 Symposium (HCS)*, pages 1–24. IEEE Computer Society, 2019.
- [20] Jacob Devlin, Ming-Wei Chang, Kenton Lee, and Kristina Toutanova. Bert: Pre-training of deep bidirectional transformers for language understanding. *arXiv preprint arXiv:1810.04805*, 2018.
- [21] Safaa Diab, Amir Nassereldine, Mohammed Alser, Juan Gómez Luna, Onur Mutlu, and Izzat El Hajj. A framework for high-throughput sequence alignment using real processing-in-memory systems. *Bioinformatics*, 39(5):btad155, 2023.
- [22] Alexey Dosovitskiy, Lucas Beyer, Alexander Kolesnikov, Dirk Weissenborn, Xiaohua Zhai, Thomas Unterthiner, Mostafa Dehghani, Matthias Minderer, Georg Heigold, Sylvain Gelly, Jakob Uszkoreit, and Neil Houlsby. An image is worth 16x16 words: Transformers for image recognition at scale. In *International Conference on Learning Representations*, 2021.
- [23] Jiarui Fang, Yang Yu, Chengduo Zhao, and Jie Zhou. Turbotransformers: an efficient gpu serving system for transformer models. In *Proceedings of the 26th ACM SIGPLAN Symposium on Principles and Practice of Parallel Programming*, pages 389–402, 2021.
- [24] Jiarui Fang, Yang Yu, Chengduo Zhao, and Jie Zhou. Turbotransformers: an efficient gpu serving system for transformer models. In *Proceedings of the 26th ACM SIGPLAN Symposium on Principles and Practice of Parallel Programming*, pages 389–402, 2021.
- [25] Amin Farmahini-Farahani, Jung Ho Ahn, Katherine Morrow, and Nam Sung Kim. Nda: Near-dram acceleration architecture leveraging commodity dram devices and standard memory modules. In *2015 IEEE 21st International Symposium on High Performance Computer Architecture (HPCA)*, pages 283–295. IEEE, 2015.
- [26] João Dinis Ferreira, Gabriel Falcao, Juan Gómez-Luna, Mohammed Alser, Lois Orosa, Mohammad Sadrosadati, Jeremie S Kim, Geraldo F Oliveira, Taha Shahroodi, Anant Nori, et al. pluto: Enabling massively parallel computation in dram via lookup tables. In *2022 55th IEEE/ACM International Symposium on Microarchitecture (MICRO)*, pages 900–919. IEEE, 2022.
- [27] Mingyu Gao, Grant Ayers, and Christos Kozyrakis. Practical near-data processing for in-memory analytics frameworks. In *2015 International Conference on Parallel Architecture and Compilation (PACT)*, pages 113–124. IEEE, 2015.
- [28] Mingyu Gao, Jing Pu, Xuan Yang, Mark Horowitz, and Christos Kozyrakis. Tetris: Scalable and efficient neural network acceleration with 3d memory. In *Proceedings of the Twenty-Second International Conference on Architectural Support for Programming Languages and Operating Systems*, pages 751–764, 2017.
- [29] Pin Gao, Lingfan Yu, Yongwei Wu, and Jinyang Li. Low latency rnn inference with cellular batching. In *Proceedings of the Thirteenth EuroSys Conference*, pages 1–15, 2018.
- [30] Georgi Gerganov. Ggml tensor library for machine learning. <https://github.com/ggerganov/ggml>.
- [31] Christina Giannoula, Ivan Fernandez, Juan Gómez-Luna, Nectarios Koziris, Georgios Goumas, and Onur Mutlu. Towards efficient sparse matrix vector multiplication on real processing-in-memory architectures. *ACM SIGMETRICS Performance Evaluation Review*, 50(1):33–34, 2022.
- [32] Christina Giannoula, Nandita Vijaykumar, Nikola Papadopoulou, Vasileios Karakostas, Ivan Fernandez, Juan Gómez-Luna, Lois Orosa, Nectarios Koziris, Georgios Goumas, and Onur Mutlu. Synchron: Efficient synchronization support for near-data-processing architectures. In *2021 IEEE International Symposium on High-Performance Computer Architecture (HPCA)*, pages 263–276. IEEE, 2021.
- [33] Juan Gómez-Luna, Izzat El Hajj, Ivan Fernandez, Christina Giannoula, Geraldo F Oliveira, and Onur Mutlu. Benchmarking a new paradigm: An experimental analysis of a real processing-in-memory architecture. *arXiv preprint arXiv:2105.03814*, 2021.
- [34] Juan Gómez-Luria, Yuxin Guo, Sylvain Brocard, Julien Legriel, Remy Cimadomo, Geraldo F Oliveira, Gagandeep Singh, and Onur Mutlu. Machine learning training on a real processing-in-memory system. In *2022 IEEE Computer Society Annual Symposium on VLSI (ISVLSI)*, pages 292–295. IEEE, 2022.
- [35] Peng Gu, Xinfeng Xie, Yufei Ding, Guoyang Chen, Weifeng Zhang, Dimin Niu, and Yuan Xie. ipim: Programmable in-memory image processing accelerator using near-bank architecture. In *2020 ACM/IEEE 47th Annual International Symposium on Computer Architecture (ISCA)*, pages 804–817. IEEE, 2020.
- [36] Kaiming He, Xiangyu Zhang, Shaoqing Ren, and Jian Sun. Deep residual learning for image recognition. In *2016 IEEE Conference on Computer Vision and Pattern Recognition, CVPR*, pages 770–778. IEEE Computer Society, 2016.
- [37] Byungchul Hong, Yeonju Ro, and John Kim. Multi-dimensional parallel training of winograd layer on memory-centric architecture. In *2018 51st Annual IEEE/ACM International Symposium on Microarchitecture (MICRO)*, pages 682–695. IEEE, 2018.
- [38] Kevin Hsieh, Eiman Ebrahimi, Gwangsun Kim, Niladrish Chatterjee, Mike O’Connor, Nandita Vijaykumar, Onur Mutlu, and Stephen W Keckler. Transparent offloading and mapping (tom) enabling programmer-transparent near-data processing in gpu systems. *ACM SIGARCH Computer Architecture News*, 44(3):204–216, 2016.

- [39] Intel. Intel 64 and ia-32 architectures software developer manual volume 3b. <https://www.intel.com/content/www/us/en/developer/articles/technical/intel-sdm.html>.
- [40] Intel. Intel advisor. <https://www.intel.cn/content/www/cn/zh/developer/tools/oneapi/advisor.html#gs.2g5qlq>.
- [41] Intel. Intel oneapi math kernel library (mkl). <https://www.intel.com/content/www/us/en/developer/tools/oneapi/onemkl.html>.
- [42] Intel. oneapi deep neural network library. <https://github.com/oneapi-src/oneDNN>.
- [43] Intel. Rapl power meter. <https://www.intel.com/content/www/us/en/developer/articles/technical/software-security-guidance/advisory-guidance/running-average-power-limit-energy-reporting.html>.
- [44] Yangqing Jia, Evan Shelhamer, Jeff Donahue, Sergey Karayev, Jonathan Long, Ross Girshick, Sergio Guadarrama, and Trevor Darrell. Caffe: Convolutional architecture for fast feature embedding. *arXiv preprint arXiv:1408.5093*, 2014.
- [45] Yifan Jiang, Shiyu Chang, and Zhangyang Wang. Transgan: Two pure transformers can make one strong gan, and that can scale up. *Advances in Neural Information Processing Systems*, 34:14745–14758, 2021.
- [46] Norman P Jouppi, Doe Hyun Yoon, Matthew Ashcraft, Mark Gottscho, Thomas B Jablin, George Kurian, James Laudon, Sheng Li, Peter Ma, Xiaoyu Ma, et al. Ten lessons from three generations shaped google’s tpuv4i: Industrial product. In *2021 ACM/IEEE 48th Annual International Symposium on Computer Architecture (ISCA)*, pages 1–14. IEEE, 2021.
- [47] Norman P Jouppi, Cliff Young, Nishant Patil, David Patterson, Gaurav Agrawal, Raminder Bajwa, Sarah Bates, Suresh Bhatia, Nan Boden, Al Borchers, et al. In-datacenter performance analysis of a tensor processing unit. In *Proceedings of the 44th annual international symposium on computer architecture*, pages 1–12, 2017.
- [48] Hongbo Kang, Yiwei Zhao, Guy E Blelloch, Laxman Dhulipala, Yan Gu, Charles McGuffey, and Phillip B Gibbons. Pim-tree: A skew-resistant index for processing-in-memory. *arXiv preprint arXiv:2211.10516*, 2022.
- [49] Hongbo Kang, Yiwei Zhao, Guy E Blelloch, Laxman Dhulipala, Yan Gu, Charles McGuffey, and Phillip B Gibbons. Pim-trie: A skew-resistant trie for processing-in-memory. In *Proceedings of the 35th ACM Symposium on Parallelism in Algorithms and Architectures*, pages 1–14, 2023.
- [50] Liu Ke, Udit Gupta, Benjamin Youngjae Cho, David Brooks, Vikas Chandra, Utku Diril, Amin Firoozshahian, Kim Hazelwood, Bill Jia, Hsien-Hsin S Lee, et al. Recnmp: Accelerating personalized recommendation with near-memory processing. In *2020 ACM/IEEE 47th Annual International Symposium on Computer Architecture (ISCA)*, pages 790–803. IEEE, 2020.
- [51] Liu Ke, Udit Gupta, Benjamin Youngjae Cho, David Brooks, Vikas Chandra, Utku Diril, Amin Firoozshahian, Kim Hazelwood, Bill Jia, Hsien-Hsin S Lee, et al. Recnmp: Accelerating personalized recommendation with near-memory processing. In *2020 ACM/IEEE 47th Annual International Symposium on Computer Architecture (ISCA)*, pages 790–803. IEEE, 2020.
- [52] Duckhwan Kim, Taesik Na, Sudhakar Yalamanchili, and Saibal Mukhopadhyay. Deeptrain: A programmable embedded platform for training deep neural networks. *IEEE Transactions on Computer-Aided Design of Integrated Circuits and Systems*, 37(11):2360–2370, 2018.
- [53] Alex Krizhevsky, Geoffrey Hinton, et al. Learning multiple layers of features from tiny images. 2009.
- [54] Yongkee Kwon, Kornijcuk Vladimir, Nahsung Kim, Woojae Shin, Jongsoon Won, Minkyu Lee, Hyunha Joo, Haerang Choi, Guhyun Kim, Byeongju An, et al. System architecture and software stack for gddr6-aim. In *2022 IEEE Hot Chips 34 Symposium (HCS)*, pages 1–25. IEEE, 2022.
- [55] Young-Cheon Kwon, Suk Han Lee, Jaehoon Lee, Sang-Hyuk Kwon, Je-Min Ryu, Jong-Pil Son, Seongil O, Hak-soo Yu, Haesuk Lee, Soo Young Kim, Youngmin Cho, Jin Guk Kim, Jongyoon Choi, Hyunsung Shin, Jin Kim, BengSeng Phuah, HyoungMin Kim, Myeong Jun Song, Ahn Choi, Daeho Kim, Sooyoung Kim, Eun-Bong Kim, David Wang, Shinhaeng Kang, Yuhwan Ro, Seungwoo Seo, Joon-Ho Song, Jaeyoun Youn, Kyomin Sohn, and Nam Sung Kim. 25.4 A 20nm 6gb function-in-memory dram, based on HBM2 with a 1.2tflops programmable computing unit using bank-level parallelism, for machine learning applications. In *IEEE International Solid-State Circuits Conference, ISSCC 2021, San Francisco, CA, USA, February 13-22, 2021*, pages 350–352. IEEE, 2021.
- [56] Youngeun Kwon, Yunjae Lee, and Minsoo Rhu. Tensordimm: A practical near-memory processing architecture for embeddings and tensor operations in deep learning. In *Proceedings of the 52nd Annual IEEE/ACM International Symposium on Microarchitecture*, pages 740–753, 2019.
- [57] Youngeun Kwon, Yunjae Lee, and Minsoo Rhu. Tensordimm: A practical near-memory processing architecture for embeddings and tensor operations in deep learning. In *Proceedings of the 52nd Annual IEEE/ACM International Symposium on Microarchitecture*, pages 740–753, 2019.
- [58] Dominique Lavenier, Remy Cimadomo, and Romaric Jodin. Variant calling parallelization on processor-in-memory architecture. In *2020 IEEE International Conference on Bioinformatics and Biomedicine (BIBM)*, pages 204–207. IEEE, 2020.
- [59] Sukhan Lee, Shin-haeng Kang, Jaehoon Lee, Hyeonsu Kim, Eojin Lee, Seungwoo Seo, Hosang Yoon, Seungwon Lee, Kyoungwan Lim, Hyunsung Shin, et al. Hardware architecture and software stack for pim based on commercial dram technology: Industrial product. In *2021 ACM/IEEE 48th Annual International Symposium on Computer Architecture (ISCA)*, pages 43–56. IEEE, 2021.
- [60] Young Sik Lee and Tae Hee Han. Task parallelism-aware deep neural network scheduling on multiple hybrid memory cube-based processing-in-memory. *IEEE Access*, 9:68561–68572, 2021.
- [61] Cong Li, Zhe Zhou, Xingchen Li, Guangyu Sun, and Dimin Niu. Nm-explorer: An efficient exploration framework for dimm-based near-memory tensor reduction. In *2023 60th ACM/IEEE Design Automation Conference (DAC)*, pages 1–6. IEEE, 2023.
- [62] Chaemin Lim, Suhyun Lee, Jinwoo Choi, Jounghoo Lee, Seongyeon Park, Hanjun Kim, Jinho Lee, and Youngsok Kim. Design and analysis of a processing-in-dimm join algorithm: A case study with upmem dimms. *Proceedings of the ACM on Management of Data*, 1(2):1–27, 2023.
- [63] Liu Liu, Jilan Lin, Zheng Qu, Yufei Ding, and Yuan Xie. Enmc: Extreme near-memory classification via approximate screening. In *MICRO-54: 54th Annual IEEE/ACM International Symposium on Microarchitecture*, pages 1309–1322, 2021.
- [64] Yinhan Liu, Myle Ott, Naman Goyal, Jingfei Du, Mandar Joshi, Danqi Chen, Omer Levy, Mike Lewis, Luke Zettlemoyer, and Veselin Stoyanov. Roberta: A robustly optimized bert pretraining approach. *arXiv preprint arXiv:1907.11692*, 2019.
- [65] Ze Liu, Yutong Lin, Yue Cao, Han Hu, Yixuan Wei, Zheng Zhang, Stephen Lin, and Baining Guo. Swin transformer: Hierarchical vision transformer using shifted windows. In *Proceedings of the IEEE/CVF international conference on computer vision*, pages 10012–10022, 2021.
- [66] Bradley McDanel, Surat Teerapittayanon, and H. T. Kung. Embedded binarized neural networks. *CoRR*, abs/1709.02260, 2017.
- [67] Lifeng Nai, Ramyad Hadidi, Jaewoong Sim, Hyojong Kim, Pranith Kumar, and Hyesoon Kim. Graphpim: Enabling instruction-level pim offloading in graph computing frameworks. In *2017 IEEE International symposium on high performance computer architecture (HPCA)*, pages 457–468. IEEE, 2017.

- [68] Vinod Nair and Geoffrey E Hinton. Rectified linear units improve restricted boltzmann machines. In *Proceedings of the 27th international conference on machine learning (ICML-10)*, pages 807–814, 2010.
- [69] Nvidia. Cublas. <https://developer.nvidia.com/cublas>.
- [70] Nvidia. Cudnn. <https://developer.nvidia.com/cudnn>.
- [71] Samsung Advanced Institute of Technology. Pimsimulator. <https://github.com/SAITPublic/PIMSimulator>.
- [72] Geraldo F Oliveira, Juan Gómez-Luna, Mohammad Sadrosadati, Yuxin Guo, and Onur Mutlu. Transpmlib: Efficient transcendental functions for processing-in-memory systems. In *2023 IEEE International Symposium on Performance Analysis of Systems and Software (ISPASS)*, pages 235–247. IEEE, 2023.
- [73] Open Neural Network Exchange (ONNX). <https://github.com/onnx/onnx>.
- [74] Angshuman Parashar, Priyanka Raina, Yakun Sophia Shao, Yu-Hsin Chen, Victor A Ying, Anurag Mukkara, Rangharajan Venkatesan, Brucec Khailany, Stephen W Keckler, and Joel Emer. Timeloop: A systematic approach to dnn accelerator evaluation. In *2019 IEEE international symposium on performance analysis of systems and software (ISPASS)*, pages 304–315. IEEE, 2019.
- [75] Jaehyun Park, Byeongho Kim, Sungmin Yun, Eojin Lee, Minsoo Rhu, and Jung Ho Ahn. Trim: Enhancing processor-memory interfaces with scalable tensor reduction in memory. In *MICRO-54: 54th Annual IEEE/ACM International Symposium on Microarchitecture*, pages 268–281, 2021.
- [76] Adam Paszke, Sam Gross, Francisco Massa, Adam Lerer, James Bradbury, Gregory Chanan, Trevor Killeen, Zeming Lin, Natalia Gimelshein, Luca Antiga, et al. Pytorch: An imperative style, high-performance deep learning library. *Advances in neural information processing systems*, 32, 2019.
- [77] D. Patterson, T. Anderson, N. Cardwell, R. Fromm, K. Keeton, C. Kozyrakis, R. Thomas, and K. Yelick. A case for intelligent ram. *IEEE Micro*, 17(2):34–44, 1997.
- [78] Alec Radford, Jeffrey Wu, Rewon Child, David Luan, Dario Amodei, Ilya Sutskever, et al. Language models are unsupervised multitask learners. *OpenAI blog*, 1(8):9, 2019.
- [79] Colin Raffel, Noam Shazeer, Adam Roberts, Katherine Lee, Sharan Narang, Michael Matena, Yanqi Zhou, Wei Li, and Peter J Liu. Exploring the limits of transfer learning with a unified text-to-text transformer. *The Journal of Machine Learning Research*, 21(1):5485–5551, 2020.
- [80] Fabian Schuiki, Michael Schaffner, Frank K Gürkaynak, and Luca Benini. A scalable near-memory architecture for training deep neural networks on large in-memory datasets. *IEEE Transactions on Computers*, 68(4):484–497, 2018.
- [81] Haichen Shen, Lequn Chen, Yuchen Jin, Liangyu Zhao, Bingyu Kong, Matthai Philipose, Arvind Krishnamurthy, and Ravi Sundaram. Nexus: A gpu cluster engine for accelerating dnn-based video analysis. In *Proceedings of the 27th ACM Symposium on Operating Systems Principles*, pages 322–337, 2019.
- [82] Purab Ranjan Sutradhar, Sathwika Bavikadi, Mark Connolly, Savankumar Prajapati, Mark A Indovina, Sai Manoj Pudukotai Dinakarrao, and Amlan Ganguly. Look-up-table based processing-in-memory architecture with programmable precision-scaling for deep learning applications. *IEEE Transactions on Parallel and Distributed Systems*, 33(2):263–275, 2021.
- [83] Purab Ranjan Sutradhar, Mark Connolly, Sathwika Bavikadi, Sai Manoj Pudukotai Dinakarrao, Mark A Indovina, and Amlan Ganguly. ppim: A programmable processor-in-memory architecture with precision-scaling for deep learning. *IEEE Computer Architecture Letters*, 19(2):118–121, 2020.
- [84] Xiaohu Tang, Yang Wang, Ting Cao, Li Lyna Zhang, Qi Chen, Deng Cai, Yunxin Liu, and Mao Yang. Lut-nn: Empower efficient neural network inference with centroid learning and table lookup. In *ACM MobiCom '23: The 29th Annual International Conference on Mobile Computing and Networking, Madrid, Spain, October 2 - 6, 2023*. ACM, 2023.
- [85] UPMEM. Upmem pim-dimm runtime library. [https://sdk.upmem.com/2023.1.0/202\\_RTL.html](https://sdk.upmem.com/2023.1.0/202_RTL.html).
- [86] UPMEM. Upmem software development kit (sdk). <https://sdk.upmem.com/>.
- [87] Ashish Vaswani, Noam Shazeer, Niki Parmar, Jakob Uszkoreit, Llion Jones, Aidan N Gomez, Ł ukasz Kaiser, and Illia Polosukhin. Attention is all you need. In I. Guyon, U. Von Luxburg, S. Bengio, H. Wallach, R. Fergus, S. Vishwanathan, and R. Garnett, editors, *Advances in Neural Information Processing Systems*, volume 30. Curran Associates, Inc., 2017.
- [88] Alex Wang, Amanpreet Singh, Julian Michael, Felix Hill, Omer Levy, and Samuel R Bowman. Glue: A multi-task benchmark and analysis platform for natural language understanding. *arXiv preprint arXiv:1804.07461*, 2018.
- [89] Wenhai Wang, Enze Xie, Xiang Li, Deng-Ping Fan, Kaitao Song, Ding Liang, Tong Lu, Ping Luo, and Ling Shao. Pyramid vision transformer: A versatile backbone for dense prediction without convolutions. In *Proceedings of the IEEE/CVF international conference on computer vision*, pages 568–578, 2021.
- [90] Yi Wang, Weixuan Chen, Jing Yang, and Tao Li. Towards memory-efficient allocation of cnns on processing-in-memory architecture. *IEEE Transactions on Parallel and Distributed Systems*, 29(6):1428–1441, 2018.
- [91] Xinfeng Xie, Zheng Liang, Peng Gu, Abanti Basak, Lei Deng, Ling Liang, Xing Hu, and Yuan Xie. Spacea: Sparse matrix vector multiplication on processing-in-memory accelerator. In *2021 IEEE International Symposium on High-Performance Computer Architecture (HPCA)*, pages 570–583. IEEE, 2021.
- [92] Zhilin Yang, Zihang Dai, Yiming Yang, Jaime Carbonell, Russ R Salakhutdinov, and Quoc V Le. Xlnet: Generalized autoregressive pre-training for language understanding. *Advances in neural information processing systems*, 32, 2019.
- [93] Penghang Yin, Jiancheng Lyu, Shuai Zhang, Stanley J. Osher, Yingyong Qi, and Jack Xin. Understanding straight-through estimator in training activation quantized neural nets. In *7th International Conference on Learning Representations, ICLR 2019, New Orleans, LA, USA, May 6-9, 2019*. OpenReview.net, 2019.
- [94] Shouyi Yin, Shibin Tang, Xinhan Lin, Peng Ouyang, Fengbin Tu, Jishen Zhao, Cong Xu, Shuangcheng Li, Yuan Xie, Shaojun Wei, et al. Parana: A parallel neural architecture considering thermal problem of 3d stacked memory. *IEEE Transactions on Parallel and Distributed Systems*, 30(1):146–160, 2018.
- [95] Li Yuan, Yunpeng Chen, Tao Wang, Weihao Yu, Yujun Shi, Zi-Hang Jiang, Francis EH Tay, Jiashi Feng, and Shuicheng Yan. Tokens-to-token vit: Training vision transformers from scratch on imagenet. In *Proceedings of the IEEE/CVF international conference on computer vision*, pages 558–567, 2021.
- [96] Dongping Zhang, Nuwan Jayasena, Alexander Lyashevsky, Joseph L Greathouse, Lifan Xu, and Michael Ignatowski. Top-pim: Throughput-oriented programmable processing in memory. In *Proceedings of the 23rd international symposium on High-performance parallel and distributed computing*, pages 85–98, 2014.
- [97] Mingxing Zhang, Youwei Zhuo, Chao Wang, Mingyu Gao, Yongwei Wu, Kang Chen, Christos Kozyrakis, and Xuehai Qian. Graphp: Reducing communication for pim-based graph processing with efficient data partition. In *2018 IEEE International Symposium on High Performance Computer Architecture (HPCA)*, pages 544–557. IEEE, 2018.
- [98] Mingxing Zhang, Youwei Zhuo, Chao Wang, Mingyu Gao, Yongwei Wu, Kang Chen, Christos Kozyrakis, and Xuehai Qian. Graphp: Reducing communication for pim-based graph processing with efficient



- data partition. In *2018 IEEE International Symposium on High Performance Computer Architecture (HPCA)*, pages 544–557. IEEE, 2018.
- [99] Susan Zhang, Stephen Roller, Naman Goyal, Mikel Artetxe, Moya Chen, Shuohui Chen, Christopher Dewan, Mona Diab, Xian Li, Xi Victoria Lin, et al. Opt: Open pre-trained transformer language models. *arXiv preprint arXiv:2205.01068*, 2022.
- [100] Ranyang Zhou, Arman Roohi, Durga Misra, and Shaahin Angizi. Red-lut: Reconfigurable in-dram luts enabling massive parallel computation. In *Proceedings of the 41st IEEE/ACM International Conference on Computer-Aided Design*, pages 1–8, 2022.
- [101] Zhe Zhou, Cong Li, Xuechao Wei, Xiaoyang Wang, and Guangyu Sun. Gnnear: Accelerating full-batch training of graph neural networks with near-memory processing. In *Proceedings of the International Conference on Parallel Architectures and Compilation Techniques*, pages 54–68, 2022.
- [102] Zhe Zhou, Cong Li, Fan Yang, and Guangyu Sun. Dimm-link: Enabling efficient inter-dimm communication for near-memory processing. In *2023 IEEE International Symposium on High-Performance Computer Architecture (HPCA)*, pages 302–316, 2023.
- [103] Zhe Zhou, Xuechao Wei, Jiejing Zhang, and Guangyu Sun. PetS: A unified framework for Parameter-Efficient transformers serving. In *2022 USENIX Annual Technical Conference (USENIX ATC 22)*, pages 489–504, Carlsbad, CA, July 2022. USENIX Association.
- [104] Youwei Zhuo, Chao Wang, Mingxing Zhang, Rui Wang, Dimin Niu, Yanzhi Wang, and Xuehai Qian. Graphq: Scalable pim-based graph processing. In *Proceedings of the 52nd Annual IEEE/ACM International Symposium on Microarchitecture*, pages 712–725, 2019.